ADVANCED MATERIALS INTERFACES
www.advmatinterfaces.de

Atomic Layer Deposition for Graphene Device Integration

*René H. J. Vervuurt, Wilhelmus M. M. (Erwin) Kessels, and Ageeth A. Bol**

Graphene is a two dimensional material with extraordinary properties, which make it an interesting material for many optical and electronic devices. The integration of graphene in these devices often requires the deposition of thin dielectric layers on top of graphene. Atomic layer deposition (ALD) is the method of choice to deposit these layers due to its ability to deposit ultra-thin, high quality films with sub-monolayer thickness control. ALD on graphene however, is a challenge due to the lack of reactive surface sites on graphene. This leads to the selective growth on grain boundaries, wrinkles and defect sites present in the graphene. In this review an overview of the different methods to achieve uniform deposition of ALD on graphene is presented. The advantages and disadvantages of each method are discussed from the perspective of ALD together with the opportunities for further research. Special emphasis is given to the recent advancements in the understanding of the ALD process conditions and their influence on the deposition uniformity on graphene. Particularly, improving the quality of the dielectric layers deposited by ALD while maintaining the pristine properties of graphene, will prove vital for the device integration of graphene.

1. Introduction

Graphene is a two-dimensional material with extraordinary properties, that has gathered considerable interest of the research community over the past few years.[1] The high charge carrier mobility of graphene combined with its good thermal conductivity, large maximum current density and the ability to absorb light over a broad spectral range make it a promising material for post-silicon electronic and optical applications.[2–4] Device integration often requires the ability to deposit ultra-thin (<10 nm) uniform high-κ dielectric layers on graphene. The high charge carrier and large maximum current density of graphene for example, make it a suitable channel material for graphene transistors where the zero band-gap of graphene is not a fundamental limitation.[3] To make top-gated radio-frequency graphene transistors the deposition of a high-κ dielectric layer on top of graphene is required for good electrostatic control of the channel, which increases device performance and improves device reliability.[5,6] The integration of graphene in lateral spin valves requires the deposition of ultra-thin dielectrics on the graphene to realize electrical spin injection,[7,8] whereas for bilayer pseudospin transistors (BiSFETs) the deposition of thin dielectrics on graphene (acting as a tunnel barrier) is essential.[9–11]

This review discusses the deposition of such ultra-thin dielectric layers on graphene by atomic layer deposition (ALD). ALD is a chemical vapor deposition (CVD) technique consisting of two self-limiting surface reactions, or half-cycles, in which the growth substrate is exposed to alternating pulses of precursor and co-reactant. These pulses are separated by pump or purge steps (**Figure 1**).[12] Each ALD cycle a (sub)monolayer of material is deposited. The cyclic nature of the ALD process makes it possible to deposit high quality materials uniformly distributed over large areas, with precise control of the layer thickness. Apart from these benefits, ALD has an additional advantage for the deposition of dielectric materials on graphene compared to other deposition methods. The commonly used physical vapor deposition (PVD) techniques such as sputtering, pulsed laser deposition and e-beam evaporation easily damage the graphene during deposition, resulting in a reduction of the graphene charge carrier mobility that reduces device performance.[13] This damage can be avoided when thermal ALD is used. This is because the absence of energetic species and reactive species, such as ions and radicals during thermal ALD.[12]

The initiation of ALD growth on graphene however, is known to be a challenge.[14] This is because graphene consists of pure sp^2 bonded carbon and therefore lacks out-of-plane bonds or surface groups needed for the initiation of ALD growth.[15,16] To overcome these nucleation issues several different surface preparation techniques to initialize ALD on graphene have been explored over the years. Apart from the many articles published, several review papers discussing the possibilities these techniques offer for the uniform ALD of dielectrics on graphene have appeared.[17–20] The most recent being from 2013. Most available reviews focus on ALD for carbon nanoelectronics in general and are device oriented.[17,19,20] So far a review focusing on the field from an ALD processing perspective has not appeared. Furthermore, since 2013, significant advances have been made in the field, especially in the understanding of the ALD process conditions and their influence on the deposition uniformity.[21,22] Also a shift in the type of graphene used has occurred. Initially, most of the work studying the growth of dielectrics by ALD on graphene focused on using exfoliated graphene flakes or highly ordered pyrolytic graphite (HOPG) as a substrate material.[14,23,24] This was because these

R. H. J. Vervuurt, W. M. M. (Erwin) Kessels, A. A. Bol
Department of Applied Physics
Eindhoven University of Technology
P.O. Box 513, 5600 MB Eindhoven, The Netherlands
E-mail: a.a.bol@tue.nl

DOI: 10.1002/admi.201700232

© 2017 WILEY-VCH Verlag GmbH & Co. KGaA, Weinheim

materials were readily available when graphene first attracted the interest of the research community and did not require additional experience in the synthesis of graphene. Only later when first epitaxial graphene and later CVD graphene became more commonly available, ALD was attempted on these graphene types.[25,26] For electronic and optical applications these last two are of significantly larger interest due to their scalability, but the work done on both exfoliated flakes and HOPG has served as an excellent starting point to better understand the nucleation of ALD growth on graphene.

ALD has also been performed on graphene which is synthesized by other methods than the ones mentioned above.[27] For example ALD was used on graphene nano-sheets or reduced graphene oxide (rGO), synthesized by chemical exfoliation.[28] Although these graphene types are of interest for electrochemical applications, the quality is too low for high end optical and electronic applications. Furthermore because the graphene created by these methods is defective and contains many functional surface groups or edges, ALD is relatively straightforward on these graphene types.[28–30] For this reason, these graphene types are not considered here unless these are used as a nucleation layer on high quality graphene to initiate ALD growth.

In this review paper, an overview of the different methods to achieve uniform deposition of ALD on graphene reported to date is presented. The advantages and disadvantages of each method are discussed from the perspective of ALD. Special emphasis is given to the recent advancements in the understanding of the ALD process conditions and their influence on the deposition uniformity on graphene. First the direct ALD of dielectrics on pristine (untreated) graphene is discussed in Section 2. In this section the influence of the graphene synthesis method on the ALD growth behavior is discussed, together with the influence of the ALD process parameters and the underlying substrate on the ability to deposit uniform ALD layers on graphene. Section 3 provides an overview of the different surface preparation techniques that can be used to initiate ALD growth on graphene; 1) the use of polymer seed-layers to initialize ALD growth, 2) the use of evaporated seed-layers and 3) the creation of functional groups on the graphene surface by plasma and ozone treatments. The review will end with a perspective for further research in Section 4.

2. ALD on Pristine Graphene

ALD on pristine graphene and HOPG is a challenge due to the lack of reactive surface sites or functional groups on graphene. As a result ALD on pristine graphene often leads to non-uniform film coverage or even the absence of film growth (**Figure 2**).[14–21] However, for graphene device integration the deposition of uniform layers on graphene is essential. Therefore approaches to carry out ALD of dielectric materials on graphene have been investigated thoroughly in literature since the discovery of its outstanding electronic properties by Geim and Noveselov in 2004.[31] An overview of the literature investigating the ALD of dielectric materials grown on graphene is given in **Table 1**. The table provides a full overview of reports addressing ALD growth on HOPG, exfoliated graphene, epitaxial graphene and CVD graphene published until recently (February 2017).

René Vervuurt earned his M.Sc. Degree in Applied Physics at the Eindhoven University of Technology in 2012. Currently René is a Ph.D. student in the plasma & materials processing group at the Eindhoven University of Technology. His doctoral thesis work focusses on the deposition of thin metal and dielectric layers on graphene by ALD for electronic applications.

Erwin Kessels is a full professor at the Eindhoven University of Technology TU/e where he is also the scientific director of the NanoLab@TU/e clean room facilities. Erwin received his M.Sc. and Ph.D. degree (cum laude) in Applied Physics from the TU/e in 1996 and 2000, respectively. His research covers the preparation of ultrathin films and nanostructures using methods such as (plasma-enhanced) chemical vapor deposition and atomic layer deposition, mostly for applications within nanoelectronics and photovoltaics.

Ageeth Bol is an associate professor of applied physics at Eindhoven University of Technology. She received her M.Sc. and Ph.D. in chemistry from Utrecht University. After obtaining her PhD degree in 2001 she worked for Philips Electronics and at the IBM TJ Watson Research Center. In 2011 she joined the Eindhoven University of Technology. Her current research interests include the fabrication, modification and integration of 1-D and 2-D nanomaterials for nanodevice applications and catalysis.

Also indicated in the table are the type of functionalization used to achieve (uniform) growth, the underlying substrate, temperature of the ALD process, minimum thickness for which a closed dielectric layer was reported and whether the graphene was damaged during the functionalization process or subsequent ALD deposition. It should be noted that almost all processes listed used a metal organic precursor combined with

 © 2017 WILEY-VCH Verlag GmbH & Co. KGaA, Weinheim

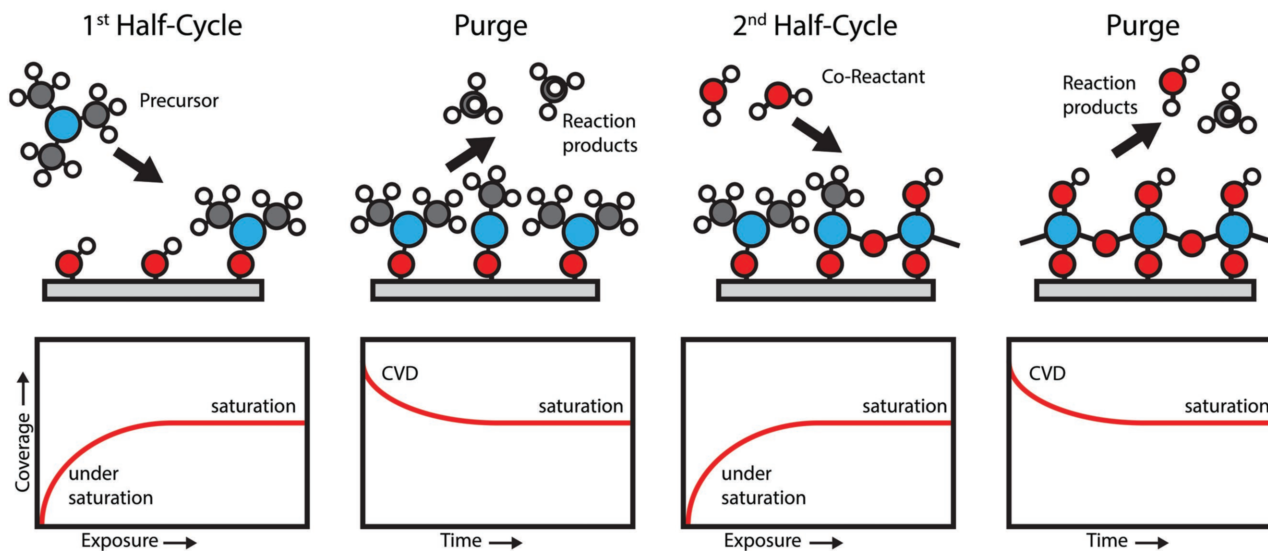

Figure 1. Schematic representation of an ALD process cycle, which consist of two half reactions. The reactants in the first half-cycle (precursor exposure) and second half-cycle (co-reactant exposure) are self-limiting, i.e. the process stops once all available surface sites have reacted. The precursor and co-reactant dose are separated by pump or purge steps to prevent unwanted gas phase reactions between the precursor and co-reactant. At the end of the second half-cycle a surface is obtained identical to the starting surface of the first half cycle. This makes it possible to obtain the desired film thickness by repeating the half-cycles in an ABAB fashion. The resulting coverage, or growth per cycle (GPC), as a function of the exposure and purge time is indicated as well. Care should be taken that the exposure steps and purge steps are sufficiently long such that saturated growth is obtained and the reaction between the precursor and the co-reactant in the gas phase is prevented (CVD growth).

H_2O as the co-reactant. Only in a few cases the co-reactant was different, namely NO_2, O_3 or an O_2 plasma, indicated by an * in the table. This is because these alternative co-reactants can easily damage the graphene, unless special precautions are taken. This will be discussed in Section 3.

H_2O based ALD processes on HOPG and graphene result most of the time in the preferential growth of the material on the defects sites, grain boundaries and wrinkles present in the graphene, as illustrated in Figure 2 for the deposition of Al_2O_3 on CVD graphene.[32] The preferential deposition on defect sites, grain boundaries and graphene wrinkles is a result of the lack of functionalized dangling bonds on the graphene basal plane. Only on defect sites and grain boundaries where functional groups are present ALD nucleation is possible.[14–16,23,24] Density functional theory (DFT) calculations have shown that various ALD precursors tend to physisorb on the graphene basal plane.[15,16,21] Chemisorption of precursor molecules on the graphene is unlikely due to the high activation barriers, typically several eV, which makes ALD nucleation difficult. Grain boundaries on the other hand often contain heptagon-pentagon or octagon-pentagon units on which precursor chemisorption is possible, see **Figure 3**.[16] The C—C bonds in these grain boundaries are strained making them more reactive towards ALD precursor adsorption. Similarly defect sites, for example mono and divacancies, are also more reactive as are defects containing epoxy or hydroxyl groups.[16] Wrinkles on the other hand do not contain additional defects or functional groups but consist of folded graphene layers. The C—C bonds present in these wrinkles are strained, which makes them more reactive.[86,87] Furthermore, photoresist residues left over from the graphene transfer process could gather at wrinkles, which could also act as a nucleation site for the subsequent ALD process. ALD growth therefore preferentially starts at defects, grain boundaries and wrinkles, whereas the pristine basal plane remains unreactive during ALD growth.

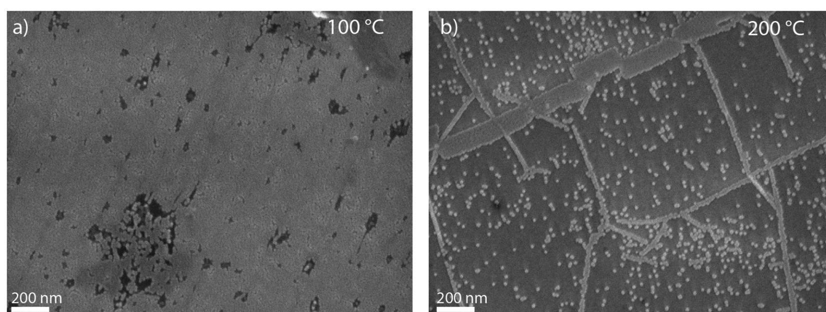

Figure 2. Scanning electron microscope (SEM) image of CVD graphene, transferred to a SiO_2 substrate, after 100 cycles of Al_2O_3 ALD. The Al_2O_3 was deposited at a) 100 °C and b) 200 °C. At 100 °C pinholes are observed throughout the Al_2O_3 layer. At 200 °C the deposition becomes more selective towards the wrinkles, defects and grain boundaries of the graphene. The difference in nucleation density can be explained by the larger amount of physisorbed H_2O being present on the graphene at lower deposition temperatures. Adapted with permission.[32] Copyright 2017, American Chemical Society.

Experimentally non-uniform ALD growth is observed for all types of graphene; HOPG,[22–26] exfoliated graphene,[14,33] CVD graphene,[26,34] and epitaxial graphene.[25] The selectivity of the ALD process towards the defect sites and grain boundaries however,

© 2017 WILEY-VCH Verlag GmbH & Co. KGaA, Weinheim

Table 1. Overview of the literature that has appeared on ALD of dielectric materials on to graphene until February 2017. The different types of *sp*^{2} materials considered are HOPG, exfoliated graphene, CVD graphene and epitaxial graphene. Listed are the type of functionalization used to achieve uniform growth, the dielectric material deposited, the graphene synthesis method, the substrate material, temperature of the ALD process, minimum thickness for which a closed layer is obtained and whether the graphene was damaged by the functionalization/ALD process. An * indicates that during the ALD process the H_2O as co-reactant is replaced by either NO_2, O_3 or O_2 plasma. A '–' means not known.

Functionalization	Dielectric	*sp*^{2} Carbon Material	Substrate	T [°C]	Thickness [nm]	Graphene Damage	Reference
None	Al_2O_3	HOPG	HOPG	RT–350	Not closed	–	[22–26]
	Al_2O_3	Exfoliated Graphene	SiO_2	100–200	Not closed	No	[14,33]
	Al_2O_3	CVD Graphene	SiO_2	80–200	Not closed	No	[26,34]
	Al_2O_3	CVD Graphene	Cu	80;200	10 (80 °C)	No	[26]
	Al_2O_3	CVD Graphene	SiO_2	150	Not closed	Yes	[35]
	Al_2O_3	CVD Graphene	Ni-Au	80	10	No	[26]
	Al_2O_3	Epitaxial Graphene	SiC	200–350	Not closed	No	[25]
	HfO_2	HOPG	HOPG	200–300	Not closed	–	[23]
	HfO_2	Exfoliated Graphene	SiO_2	250	Not closed	–	[21]
	HfO_2	Exfoliated Graphene	SiO_2	110	30	No	[36]
	HfO_2	Exfoliated Graphene	SiO_2	90	5	No	[37]
	HfO_2	CVD Graphene	SiO_2	250	Not closed	No	[21]
	HfO_2	Epitaxial Graphene	SiC	110	>25	No	[38]
	ZnO	CVD Graphene	SiO_2	300	Not closed	No	[39]
	ZrO_2	CVD Graphene	QCM Sensor	190	–	Yes	[40]
Long precursor dose	Al_2O_3	HOPG	HOPG	200	Not closed	–	[22]
	Al_2O_3	CVD Graphene	SiO_2	200	Not closed	No	[22]
	Al_2O_3	CVD Graphene	Ge	200	Not closed	No	[22]
	Al_2O_3	CVD Graphene	Cu	200	1.2	No	[22]
	Al_2O_3	CVD Graphene	Al_2O_3	100:250	22	No	[41]
No purge steps	Al_2O_3	CVD Graphene	SiO_2	100	10	No	[42]
SAM (PTCA)	Al_2O_3	Exfoliated Graphene	SiO_2	100	2.8 excluding SAM	–	[14]
	ZnO	CVD Graphene	SiO_2	120	60 excluding SAM	No	[43]
SAM (PTCDA)	Al_2O_3	Exfoliated Graphene	SiO_2	150	10	No	[6]
	Al_2O_3	Epitaxial Graphene	SiC	100	3	–	[44]
	Al_2O_3	Epitaxial Graphene	SiC	150	10	–	[6]
	HfO_2	Epitaxial Graphene	SiC	100	3	–	[44]
	HfO_2	Epitaxial Graphene	SiC	150	10	–	[6]
SAM (FDTS)	HfO_2	CVD Graphene	SiO_2	400	10	No	[45]
SAM (4MP)	ZnO	Exfoliated Graphene	SiO_2	80	2 excluding SAM	No	[46]
SAM (HMDS)	Al_2O_3	CVD Graphene	SiO_2	125	Not closed	No	[47]
SAM (HMDS) + Air Exposure	Al_2O_3	CVD Graphene	SiO_2	125	Not closed	No	[47]
SAM (TiOPc)	Al_2O_3	HOPG	SiO_2	100	4	–	[48]
SAM (TiOPc)	Al_2O_3	CVD Graphene	SiO_2	100	4	–	[48]
Polymer (PVP)	Al_2O_3	CVD Graphene	SiO_2	–	25 including polymer (5)	No	[5]
Polymer (NFC 1400-3CP)	HfO_2	Exfoliated Graphene	SiO_2	125	20 including polymer (10)	No	[49]
	HfO_2	Exfoliated Graphene	SiO_2	200	19 including polymer (9)	–	[2]
	HfO_2	Epitaxial Graphene	SiC	–	10 excluding polymer	No	[50]
Polymer (NMP)	HfO_2	CVD Graphene	SiO_2	200	Not closed	No	[51]
Polymer (PVA) + O_3	HfO_2	Exfoliated Graphene	SiO_2	150	7.5 including polymer (2.5)	–	[52]
Al e-beam	Al_2O_3	HOPG	HOPG	200	–	–	[53]

© 2017 WILEY-VCH Verlag GmbH & Co. KGaA, Weinheim

Table 1. Continued.

Functionalization	Dielectric	sp^2 Carbon Material	Substrate	T [°C]	Thickness [nm]	Graphene Damage	Reference
	Al_2O_3	Exfoliated Graphene	SiO_2	–	15	–	[10]
	Al_2O_3	Exfoliated Graphene	SiO_2	–	25	–	[54]
	Al_2O_3	Exfoliated Graphene	SiO_2	250	10	–	[55]
	Al_2O_3	CVD Graphene	SiO_2	150	90	No	[56]
	Al_2O_3	Epitaxial Graphene	SiC	300	30 excluding seed-layer (1)	No	[57]
	Al_2O_3	Epitaxial Graphene	SiC	120	27 including seed-layer (3)	–	[58]
	Al_2O_3	Epitaxial Graphene	SiC	300	≈20	Yes	[59]
	HfO_2	Exfoliated Graphene	SiO_2	200	1.5 evaporated layer thickness	Yes	[60]
	HfO_2	Exfoliated Graphene	SiO_2	200	10	Yes	[49]
Ti e-beam	Al_2O_3	Exfoliated Graphene	SiO_2	250	2.6	–	[55]
	Al_2O_3	Epitaxial Graphene	SiC	300	≈20	Yes	[38]
	TiO_2	Epitaxial Graphene	SiC	150;300	≈20	No	[38]
Hf e-beam	HfO_2	HOPG	HOPG	200	–	–	[53]
	HfO_2	CVD Graphene	SiO_2	200	18.7 including seed-layer (3)	Yes	[51]
	HfO_2	Epitaxial Graphene	SiC	110	≈20	No	[38]
Ta e-beam	Ta_2O_5	Epitaxial Graphene	SiC	120;250	≈20	Yes	[38]
SiO_2 e-beam	Al_2O_3	CVD Graphene	SiO_2	–	20 including seed-layer (5)	Yes	[61]
	HfO_2	Epitaxial Graphene	SiC	250	12 including seed-layer (2)	Yes	[59]
Al_2O_3 e-beam	Al_2O_3	Epitaxial Graphene	SiC	300	10 including seed-layer (2)	No	[59]
	HfO_2	Epitaxial Graphene	SiC	250	10 including seed-layer (2)	No	[59]
HfO_2 e-beam	Al_2O_3	Epitaxial Graphene	SiC	300	10 including seed-layer (2)	No	[59]
	HfO_2	Epitaxial Graphene	SiC	250	10 including seed-layer (2)	No	[59]
Sputtered ZnO	HfO_2	CVD Graphene	SiO_2	200	17.1 including seed-layer (3)	Yes	[51]
O_3	Al_2O_3*	HOPG	HOPG	200	10	–	[24]
	Al_2O_3*	HOPG	HOPG	200	20	No	[62]
	Al_2O_3*	HOPG	HOPG	30; 200	Not closed	–	[63]
	Al_2O_3	HOPG	HOPG	225	Not closed	Yes	[64]
	Al_2O_3*	HOPG	HOPG	30; 200	Not closed	–	[65]
	Al_2O_3*	HOPG	HOPG	200–350	50	–	[25]
	Al_2O_3*	Exfoliated Graphene	SiO_2	25; 200	15	Temperature dependent	[66]
	Al_2O_3	Exfoliated Graphene	SiO_2	25; 150	4.5	Temperature dependent	[67]
	Al_2O_3*	CVD Graphene	Ni	80	0.6	No	[8]
	Al_2O_3	CVD Graphene	SiO_2	80;120	90	No	[68]
	Al_2O_3	Epitaxial Graphene	SiC	200–350	50	Yes	[25]
NO_2	Al_2O_3*	HOPG	HOPG	150	3	–	[69]
	Al_2O_3*	Exfoliated Graphene	SiO_2	250	12	Yes	[70]
	Al_2O_3*	Exfoliated Graphene	SiO_2	25; 225	30	–	[71]
	Al_2O_3*	Exfoliated Graphene	Free standing	180	2.8	–	[72]
	HfO_2*	Exfoliated Graphene	SiO_2	200	10	Yes	[49]
N_2 plasma	Al_2O_3	CVD Graphene	SiO_2	–	28	Yes	[73]
O_2 plasma	Al_2O_3*	CVD Graphene	SiO_2	100	9	Yes	[74]
	Al_2O_3*	CVD Graphene	SiO_2	250	5.5	Yes	[75]
	Al_2O_3	CVD Graphene	SiO_2	250	–	–	[76]

© 2017 WILEY-VCH Verlag GmbH & Co. KGaA, Weinheim

Table 1. Continued.

Functionalization	Dielectric	sp^2 Carbon Material	Substrate	T [°C]	Thickness [nm]	Graphene Damage	Reference
	Al_2O_3	CVD Graphene	SiO_2	150	4	No	[77]
	HfO_2	CVD Graphene	SiO_2	250	–	–	[76]
	HfO_2*	CVD Graphene	SiO_2	250	5.9	Yes	[75]
H_2 plasma	Al_2O_3	CVD Graphene	SiO_2	100	8	No	[32]
GO	Al_2O_3	CVD Graphene	SiO_2	–	20	No	[78]
	Al_2O_3	Epitaxial Graphene	SiC	280	4 excluding GO (1.5)	No	[79]
	HfO_2	Epitaxial Graphene	SiC	175	4 excluding GO (1.5)	No	[79]
	TiO_2	Epitaxial Graphene	SiC	300	6 excluding GO (1.5)	No	[79]
Atomic oxygen*	ZnO	Epitaxial Graphene	SiC	25;100	Not closed	No	[80]
XeF_2	Al_2O_3	Epitaxial Graphene	SiC	225	15	No	[81]
H_2O soaking	Al_2O_3	Exfoliated Graphene	SiO_2	200	10	No	[33]
	Al_2O_3	CVD Graphene	SiO_2	200	10	No	[33]
H_2O pulsing	Al_2O_3	CVD Graphene	SiO_2	100	9	No	[82,83]
	Al_2O_3	CVD Graphene	SiO_2	120	90	No	[68]
	HfO_2	CVD Graphene	SiO_2	100	9	No	[83]
	ZnO	CVD Graphene	Cu	100	>10	No	[84]
Wet chemistry	Al_2O_3	Epitaxial Graphene	SiC	200	≈25	No	[85]
Air exposure	Al_2O_3	CVD Graphene	SiO_2	125	Not closed	No	[47]

SAM: self-assembled monolayer, PTCA: 3,4,9,10-perylene tetracarboxylic acid, PTCDA: perylene-3,4,9,10-tetracarboxylic dianhydride, TiOPc: titanyl phthalocyanine, NFC 1400–3CP: polyhydroxystyrene derivative, 4MP: 4-mercaptophenol, GO: graphene oxide and FDTS: perfluorodecyltrichlorosilane, PVP: poly(4-vinylphenol), PVA: poly(vinyl alcohol), NMP: N-methyl-2-pyrrolidone and HDMS: hexamethyldisilazane.

does depend on the type of graphene and on the ALD process conditions, such as substrate temperature, the type of precursor used and the precursor dose and purge times. Each of these aspects will be discussed in more detail in the following sections.

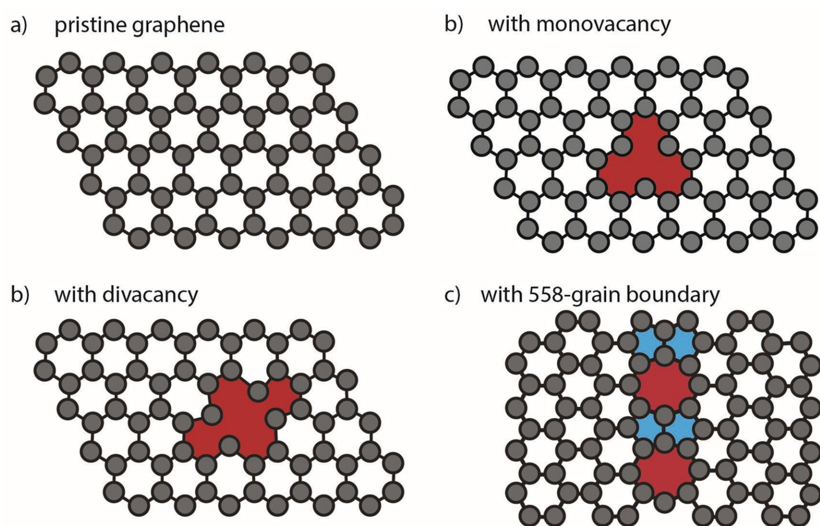

Figure 3. Top view of a) pristine graphene and b), c), d) typical graphene defects such as monovacancies, divacancies and grain boundaries. At the defects sites dangling bonds or other functional groups are present which enables the adsorption of ALD precursor molecules on these sites.[16]

2.1. Influence of the Graphene Synthesis and Transfer Method

The synthesis method of the sp^2 carbon material is of importance for the ALD nucleation and can result in different nucleation behaviors being observed. Oh et al. showed that HfO_2 nucleates much faster on CVD graphene compared to exfoliated graphene, due to the higher amount of defects and wrinkles being present for CVD graphene.[21] Apart from the higher amount of defects, CVD graphene is typically also less clean compared to exfoliated graphene, which is a result of the CVD synthesis and transfer method. CVD graphene is typically grown on a metal substrate (Cu or Ni) and transferred to the desired substrate using poly(methyl methacrylate) (PMMA) as a support layer. It is difficult to fully remove the PMMA from the graphene surface, typically some residues are left behind.[88] These residues can enhance the nucleation of the ALD process on graphene, but blocking the ALD growth is also possible. The Pt ALD precursor methylcyclopentadienyltrimethyl-platinum ($MeCpPtMe_3$) for example does not nucleate on PMMA,[15,89] and therefore might make the nucleation on graphene with PMMA residues more difficult.

 © 2017 WILEY-VCH Verlag GmbH & Co. KGaA, Weinheim

The surface cleanliness thus can lead to differences observed between the nucleation of ALD on the different graphene types, but differences are possible also between graphene samples synthesized by the same method. Prikle et al. studied the effect of the HOPG surface cleanliness on the uniformity of the ALD deposition of Al_2O_3.[65] HOPG samples were annealed before ALD to remove contaminants and adsorbates from the HOPG surface. This resulted in a much lower nucleation density compared to a freshly exfoliated or H_2O rinsed HOPG surface. A difference was observed for deposition temperatures up to 200 °C, which indicates that even at high temperatures adsorbates can remain on the graphene surface and influence the ALD nucleation. Similarly, Kim et al. observed nucleation differences for CVD transferred to SiO_2 using different methods, a cleaner the transfer method resulted in a lower the ALD nucleation density.[35] The quality of the graphene and surface cleanliness should therefore always be taken into account when comparing ALD on different graphene types. Exfoliated graphene and HOPG are generally cleaner than epitaxial and CVD graphene. Additionally the exposure of the graphene to air leads to the adsorption of impurities on the graphene surface, which can influence the ALD nucleation. Jeon et al. obtained a more uniform nucleation of Al_2O_3 on graphene if the sample was taken out of the ALD system and exposed to air every 17 cycles for a total of 69 cycles instead of growing 69 continuous cycles of Al_2O_3 on graphene.[47] This shows the adsorbed impurities from the air can enhance the ALD nucleation. Also other processing steps such as photo or electron beam lithography might result in additional residues on graphene, which can influence the ALD nucleation. Some of these steps might be difficult to avoid, but possible effects on the ALD nucleation should be taken into account. To increase reproducibility, procedures such as cleaning the graphene with a high temperature anneal (e.g. 400 °C) to reduce the amount of contaminants can be considered.

2.2. Influence of the ALD Deposition Temperature

The deposition temperature also plays an important role on the ALD nucleation on graphene. Physisorbed species tend to desorb at higher processing temperatures, whereas chemisorbed species are stable over a much wider temperature range. In the case of H_2O based ALD recipes, lower deposition temperatures (≈100 °C) generally result in a more uniform ALD nucleation on graphene.[26] This is also shown in Figure 2, where 100 cycles of Al_2O_3 was deposited on graphene at a temperature of 100 °C and 200 °C. A higher Al_2O_3 surface coverage is obtained for the lower deposition temperature. H_2O tends to physisorb on graphene at these lower temperatures, making it more difficult to remove in the subsequent purge or pump steps. The physisorbed H_2O layer reacts in the subsequent ALD cycle with the trimethylaluminum (TMA) precursor, resulting in a more uniform deposition. The use of a lower deposition temperature and sufficient ALD cycles to achieve uniform ALD growth on graphene was studied by Zou et al. and Robinson et al. who both showed that for depositing HfO_2 on either exfoliated or epitaxial graphene at 110 °C a closed layer can be obtained after the deposition of approximately 30 nm of material.[36,38] Layers thinner than 30 nm however, did not show uniform HfO_2 coverage.

Despite the advantage a lower deposition temperatures offers, the deposition temperature cannot be lowered indefinitely. This is because also the quality of the deposited high-k dielectric is of importance, While there are also other limitations, such as the ALD growth window. A lower deposition temperature often leads to the incorporation of impurities and an increase of the hydrogen content in the form of hydroxyl groups, due to the lower reactivity of the H_2O. This reduces the dielectric constant of the material deposited.[90] Furthermore, at temperatures below 100 °C H_2O is generally difficult to remove from the ALD system, requiring long purge times to avoid unwanted CVD reactions.

In some cases the uniformity of the ALD deposition can increase with deposition temperature, depending on the reactivity of the precursor molecules. Xuan et al. for example, showed that the deposition uniformity of Al_2O_3 and HfO_2 on HOPG can be increased by using a higher deposition temperature (**Figure 4**).[23] Films deposited at 200 °C still resulted in the selective deposition on the step edges of the HOPG for both Al_2O_3 and HfO_2 ALD, while on the basal plane no growth was obtained. However, when the deposition temperature was increased to 250 °C very rough, but closed HfO_2 films were deposited over the entire HOPG surface. For Al_2O_3 ALD this occurred at a temperature of 300 °C. The increase in the uniformity is caused by the reaction of one or more of the precursor molecules ($HfCl_4$, TMA or H_2O) with the sp^2 basal plane of the graphene.[38] This was confirmed using X-ray photoelectron spectroscopy (XPS) for HfO_2 ALD, which showed the formation of Hf-C bonds, at the interface between the HfO_2 and HOPG.[53] Similarly the TMA is likely to react with the HOPG surface at 300 °C. Despite the higher nucleation density obtained, the deposition of HfO_2 at these high temperatures has been shown to severely damage the graphene.[38] In the ideal case one would therefore like to deposit the dielectric on the graphene at a temperature at which the best properties are obtained for the material being deposited, while still obtaining uniform ALD growth on graphene and keeping the graphene intact.

2.3. Influence of the ALD Precursor Chemistry

The reactivity of grain boundaries, defects, wrinkles and the graphene basal plane towards ALD nucleation depends on the precursor used. The Pt precursor $MeCpPtMe_3$ for example is much more reactive towards grain boundaries than the Al_2O_3 TMA ($Al(CH_3)_3$) precursor.[15] The presence of certain ligands in the precursor can increase the adsorption energies significantly. Aromatic acetylacetonate (acac, $C_5H_7O_2$) ligands have been shown to increase the physisorption of $Pt(acac)_2$ compared to $MeCpPtMe_3$ on graphene, likely due to π–stacking interactions between the graphene and the acac ligand.[16] Evidently, it is important to consider the precursor ligands when choosing a precursor for ALD on graphene.

The influence of the precursor chemistry on the nucleation behavior of HfO_2 was also investigated by Oh et al.[21] Both $HfCl_4$ and tetrakis(dimethylamino)hafnium (TDMAH,

© 2017 WILEY-VCH Verlag GmbH & Co. KGaA, Weinheim

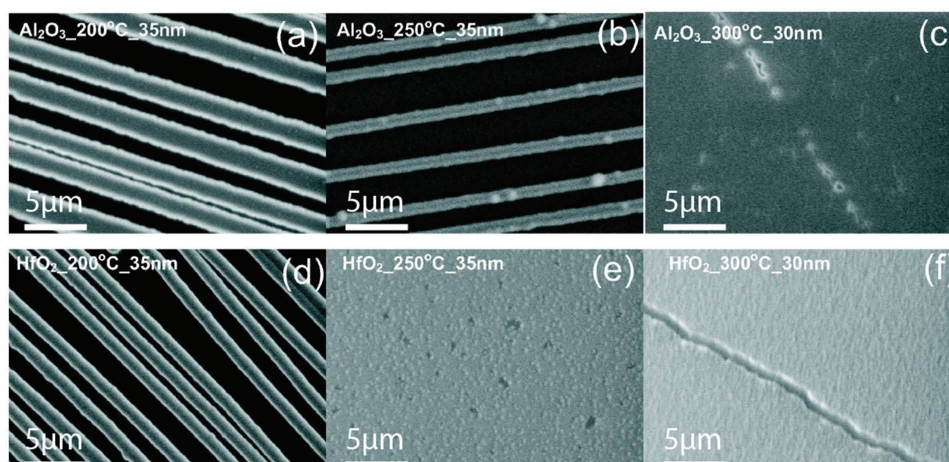

Figure 4. SEM images of Al_2O_3 ALD on HOPG deposited at a) 200 °C, b) 250 °C and c) 300 °C and HfO_2 ALD on HOPG deposited at d) 200 °C, e) 250 °C and f) 300 °C. For both HfO_2 and Al_2O_3 a more uniform growth is obtained at higher temperatures as a result of a reaction of the sp^2 bonded carbon with the ALD precursor molecules. The films however, are very rough and contain pinholes and cracks. Adapted with permission.[23] Copyright 2008, AIP Publishing.

($(CH_3)_2N)_4Hf$) were used to deposit HfO_2 films on exfoliated and CVD graphene using H_2O as the co-reactant at a substrate temperature of 250 °C. After 90 ALD cycles, HfO_2 covered 75% of the graphene surface when $HfCl_4$ was used as the Hf precursor, whereas only 35% of the surface was covered when TDMAH was used. DFT modeling showed that the physisorption of $HfCl_4$ on graphene is stronger compared to TDMAH, leading to an enhanced nucleation for $HfCl_4$. The results of Oh et al. indicate that the precursor chemistry plays an important role in the nucleation of ALD on graphene. Despite the advantages that a different precursor molecule might add, the number of types of precursors (for the same material) that have been tested in the literature is limited. This is because, apart from an advantageous adsorption on graphene, the precursor must satisfy many other requirements to be suitable for ALD processing, such as a high vapor pressure, good thermal stability and low cost, which limits the number of precursors available. In the case of Al_2O_3 for example, in all work published ALD on graphene TMA was used as the precursor. The robustness of the TMA-based ALD recipe and low cost of the precursor hamper the development and availability of alternative Al precursors that might be more suited for ALD on graphene.

2.4. Influence of the ALD Dose and Purge Times

The lack of reactive surface groups on the graphene plane means that ALD precursor adsorption mostly relies on physisorption of the precursor molecules and co-reactant. Work by McDonnel et al. showed that increasing the precursor purge time from 30 s to 300 s the amount of Al_2O_3 deposited on HOPG was decreased significantly, while no change was observed for a Si witness sample.[63] The difference between the different samples and purge times, was attributed to the physisorption of the precursor and reactant on the HOPG surface. When a longer purge time is used more of the precursor desorbs from the graphene surface, resulting in less material being deposited. A similar effect was observed by Aria et al. who instead of changing the purge times, increased the TMA precursor dose times (>2 s) while keeping the purge times constant.[22] Longer dose times resulted in more uniform nucleation on HOPG and CVD graphene. The longer exposure to the precursor most likely resulted in an increase of the physisorbed species on the graphene surface. Because the purge times were kept constant, more molecules remained on the graphene after the purge step with increasing dose times, leading to an enhanced nucleation density and the deposition of a closed graphene layer after 12 cycles for the optimized conditions (i.e. by also exploiting the influence of the underlying graphene substrate on the ALD nucleation, which will be discussed in Section 2.5). Park et al. removed the purge times during the first few ALD cycles.[42] A closed Al_2O_3 layer of approximately 10 nm was deposited in this case. The complete removal of the purge times from the ALD process however, also results in unwanted CVD reactions occurring in the gas phase, which could lead to the deposition of non-uniform films.

The use of longer precursor doses does not necessarily lead to a more uniform deposition. An example of this is shown in **Figure 5**. The figure shows the deposition of Pt by ALD on CVD graphene grown on Cu foil. The Pt was deposited using $MeCpPtMe_3$ precursor and O_2 gas as co-reactant at a temperature of 300 °C.[91] Increasing the pressure of the co-reactant (effectively increasing the O_2 dose) results in a more selective deposition towards the wrinkles and grain boundaries of the graphene, most likely due to the diffusion of Pt. Pt is known to diffuse on surfaces by a process called ripening, which is dependent on the O_2 pressure.[92,93] At higher oxygen doses, increasing amounts of the Pt surface species are converted to PtO_x which have a higher diffusion rate.[93,94] This leads to an increased Pt diffusion over the graphene surface for larger O_2 doses allowing the Pt to diffuse to grain boundaries and wrinkles of graphene, which are energetically more favorable adsorption sites compared to the graphene basal plane.[16] The diffusivity of the precursor molecules on graphene can

 © 2017 WILEY-VCH Verlag GmbH & Co. KGaA, Weinheim

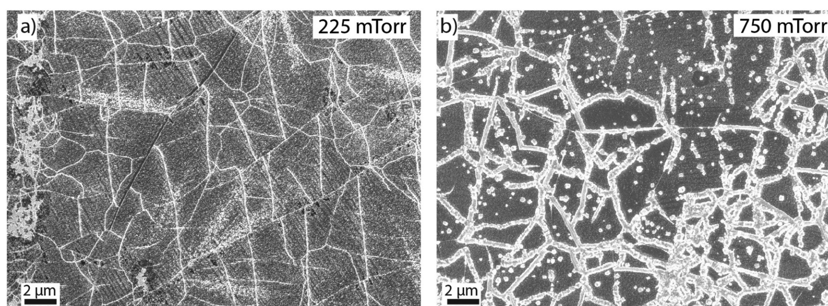

Figure 5. SEM micrograph of graphene grown on Cu foil after 500 cycles of Pt ALD at 300 °C. The Pt was deposited using $MeCpPtMe_3$ precursor and O_2 gas as co-reactant. The O_2 pressure was varied a) 225 mTorr and b) 750 mTorr. A more uniform Pt deposition can be observed for the lower O_2 pressure (the density of Pt particles in-between the grain boundaries and wrinkles goes is reduced with increasing O_2 pressure).

therefore strongly influence the ALD nucleation behavior. A similar effect has been observed for the deposition of Al_2O_3 using an Al or Ti seed-layer (see Section 3.2).

2.5. Influence of the Underlying Substrate

Apart from the ALD process parameters and the cleanliness of the graphene surface the underlying substrate also plays an important role in the nucleation of ALD films on graphene, as was shown by Dublak et al.[26] The deposition of 100 cycles of Al_2O_3 on HOPG and CVD graphene transferred to SiO_2 without any pretreatment did not result in the growth of a uniform layer, see **Figure 6**a. However, when the CVD graphene was present on a Cu substrate, uniform deposition of Al_2O_3 on graphene was obtained (Figure 6b). Similarly, using Ni-Au as the underlying substrate led to a uniform film of Al_2O_3 on graphene.[26] However, when multi-layer graphene was used on the same substrates the growth was similar to that on the HOPG and SiO_2 substrates. The enhanced nucleation when a metallic substrate was used, was ascribed to the formation of polar traps on the graphene surface due to the interaction of the metal with the graphene.[26,95] The adsorption of H_2O molecules was increased due to the presence of these polar traps resulting in the uniform nucleation of Al_2O_3 on graphene.

For non-H_2O processes the underlying substrate can also be of importance for the nucleation, as is demonstrated in **Figure 7**, which demonstrates the deposition of Pt on graphene supported by Si nano pillars and free-standing graphene, in the gap between the pillars. A higher Pt nucleation density is observed for the graphene supported by the Si pillars compared to the free standing graphene. Although the precise cause for this enhanced nucleation behavior is not yet fully understood, it shows that the interaction between the graphene and the substrate can strongly influence the ALD nucleation. The appropriate choice of substrate thus makes it possible to obtain closed layers that are significantly thinner than when the standard silicon oxide substrate is used. This can also be observed in Table , 1: For semiconductor and metal substrates generally a closed layer is obtained at lower thicknesses compared to an oxide substrate using the same functionalization process. For many applications however, the choice in substrates is limited and this effect can therefore not always be exploited.

Summarizing, the direct deposition of dielectric layers and metals on graphene by ALD does not result in uniform film growth, but in the selective deposition on the graphene grain boundaries, defects and wrinkles. The selective growth is a result of the lack of out of-plane bonds on the graphene, due to its sp^2 C configuration. Because the precursor molecules physisorb on the graphene instead of chemically bonding to the graphene, the ALD process conditions such as substrate temperature, pump times, purge times and the precursor chemistry strongly affect the deposition uniformity. The appropriate choice of precursor and substrate, as well as increasing the dose times, shortening the purge times and lowering the deposition temperature can increase the nucleation uniformity. Despite numerous efforts to optimize the process conditions, obtaining closed dielectric layers <10 nm is still troublesome and for many applications changing the substrate is not

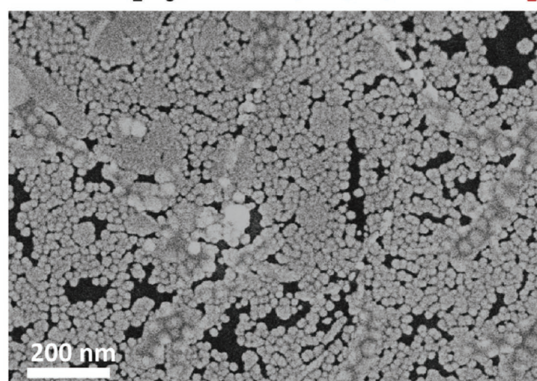

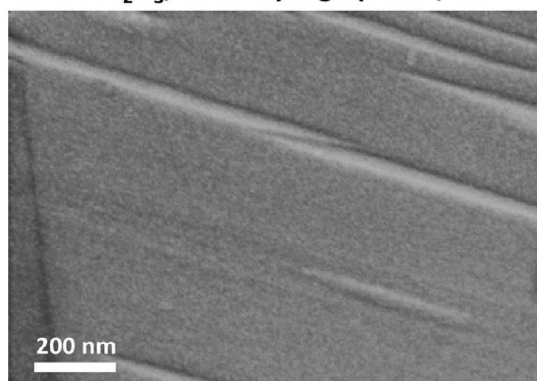

Figure 6. SEM image of the ALD growth of 10 nm Al_2O_3 at 80 °C on graphene using a) SiO_2 as the underlying substrate and b) Cu as the underlying substrate. The use of SiO_2 as the underlying substrate does not result in uniform Al_2O_3 growth on graphene, However, when Cu is used as the underlying substrate uniform ALD of Al_2O_3 deposition is observed. Adapted with permission.[26] Copyright 2012, AIP Publishing.

© 2017 WILEY-VCH Verlag GmbH & Co. KGaA, Weinheim

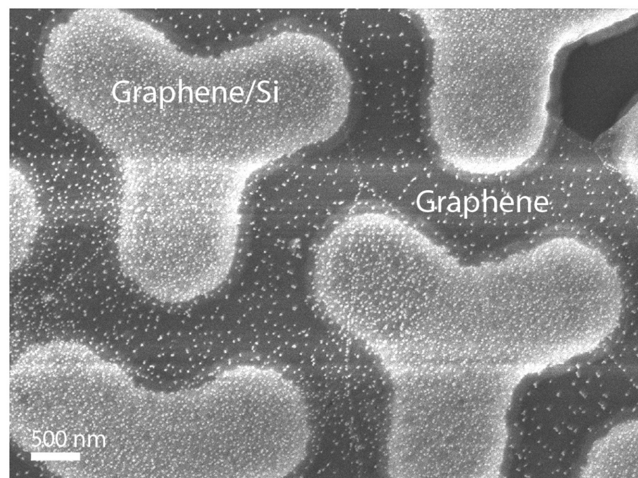

Figure 7. 500 cycles of Pt ALD on graphene transferred to Si pillars. The graphene in between the nano pillars is free-standing, i.e. not supported by a substrate. An increased nucleation density can be observed on the Graphene/Si nano pillars compared to the free standing graphene.

an option. Furthermore, the strong dependence on process conditions does not provide the best solution when reproducible results are required. To this extent the creation of functional groups on the graphene surface to enhance the nucleation of ALD on graphene has been studied extensively throughout literature and will be discussed in the next section.

3. Uniform ALD on Graphene through Surface Preparation

To enable uniform ALD on graphene the creation of functional groups on graphene has appeared to be essential. The functional groups provide adsorption sites on which the precursor molecules can chemisorb resulting in ALD of uniform films on the graphene surface. The functional groups can be created directly on the graphene itself or by the deposition of a seed-layer on the graphene. The creation of functional groups directly on the graphene can be achieved by, for example, an O_2 plasma treatment. The plasma treatment converts part of the sp^2 bonds to out-of-plane sp^3 bonds and leads to the attachment of oxygen containing surface groups. The disruption of the sp^2 backbone of the graphene by these treatments however, results in the deterioration of the electrical properties of the graphene, such as the charge carrier mobility. The use of seed-layers avoids changing the sp^2 structure of the graphene. However in this case one faces other challenges such as a lower dielectric material quality or an increase in the equivalent oxide thickness (EOT) due to the low dielectric constant of the seed-layer.

The various methods used to initialize ALD growth on graphene, shown in Table 1, can be roughly be divided into four categories; 1) the deposition of polymer seed-layers on the graphene such as self-assembled monolayers (SAMs), 2) the evaporation of metal or metal-oxide seed-layers on the graphene, 3) the creation of functional groups directly on the graphene by plasma or reactive gas functionalization, and 4) the use of wet-chemical treatments such as RCA cleaning or dipping the graphene in H_2O before processing. Each of these methods will be discussed in more detail below.

3.1. Polymer Seed-Layers

The use of polymer seed-layers to achieve uniform growth on graphene was first investigated by Wang et al. who used 3,4,9,10-perylene tetracarboxylic acid (PTCA), a SAM, to obtain uniform Al_2O_3 layers (2.8 nm thick) on graphene, as shown in **Figure 8**.[14] To cover the graphene with PTCA, graphene flakes were immersed in a PTCA solution for approximately half an hour. The PTCA contains carboxylate terminated groups which served as adsorption sites for the TMA precursor. Although not investigated, it is suggested that damage to the graphene is prevented by the non-covalent bonding of the PTCA to the graphene. Along with PTCA several other SAMs have been used to obtain uniform Al_2O_3, HfO_2 and ZnO layers on graphene such as perylene-3,4,9,10-te tracarboxylic dianhydride (PTCDA),[6,44] perfluorodecyltrichlorosilane (FDTS),[45] and 4-mercaptophenol (4MP).[51] The use of Hexamethyldisilazane (HMDS) as a seed-layer led to the deposition of non-uniform Al_2O_3 films,[47] possibly because of the hydrophobic nature of the functional groups, which decreased the adsorption of H_2O on the HDMS treated graphene surface.

Polymer seed-layers are typically deposited on the graphene by spin coating and are typically between 5–10 nm thick. Farmer et al. used the polymer NFC 1400-3CP (a polyhydroxystyrene derivative) to initiate the ALD growth of uniform 10 nm thick layers of HfO_2 on graphene.[49] After ALD, top gated field effect transistors (FETs) where made. The FET devices showed that the charge carrier mobility of the graphene decreased ≈15% after polymer deposition and subsequent HfO_2 ALD. Further analysis showed that additional phonon

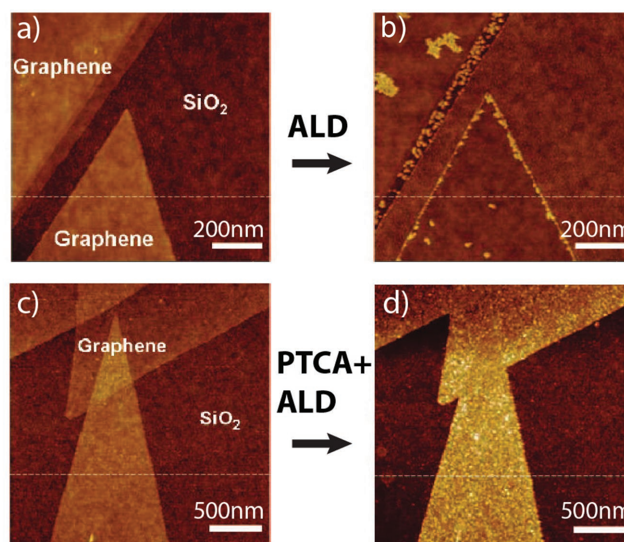

Figure 8. Atomic force microscope (AFM) images of pristine graphene a) before and b) after Al_2O_3 ALD and of PTCA functionalized graphene c) before and d) after PTCA treatment and ALD. Adapted with permission.[14] Copyright 2008, American Chemical Society.

 © 2017 WILEY-VCH Verlag GmbH & Co. KGaA, Weinheim

scattering introduced by the polymer layer was the most likely cause for the observed reduction of the mobility. Apart from a small reduction in the carrier mobility the polymer buffer layer also lead to strong p-doping of the graphene. This resulted in a 42.5 V shift in the Dirac voltage which decreased to 13.3 V after HfO_2 ALD. The doping of the graphene by the polymer buffer layer can be reduced by the appropriate choice of the polymer layer, as was shown by Shin et al. who used poly(4-vinylphenol) to obtain uniform (25 nm thick) Al_2O_3 layers on graphene, which reduced the Dirac point shift to ≈1.5 V. Both Sangwan et al.[6] and Shin et al.[78] showed that the use of a polymer seed-layer or SAM also enhances the reproducibility of devices made compared to devices where no seed-layer is used. The increased device reproducibility is likely caused by the more uniform ALD on the seed-layer as compared to the non-functionalized graphene devices. Device reliability test by Sangwan et al. showed that using Al_2O_3 as a buffer layer between the HfO_2 gate and polymer resulted in superior performance compared to devices that only used HfO_2 as a gate dielectric. Further analysis showed that the PTCDA seeded the Al_2O_3 growth more effectively than the HfO_2 growth.

All reported SAMs and other polymeric seed-layers have a limited influence on the graphene properties. Furthermore, fabricated devices show good reproducibility and therefore are a promising method to achieve uniform dielectric layers on graphene. However, there are some hurdles that need to be overcome to make polymer buffer layers or SAMs suited for future device integration. The tested SAMs and other polymers all have a relatively low dielectric constant, which together with the relatively large thickness of the films limits the minimum EOT of the gate dielectric. For example a 9 nm NFC 1400-3CP seed-layer has a dielectric constant of ≈2.5 resulting in a EOT of 14 nm for the polymer layer alone. Reducing the EOT thickness is essential for the further improvement of graphene devices. Meric et al. have shown that by using poly-vinyl alcohol (PVA), a polymer with a relatively high dielectric constant (≈6), the EOT can be reduced significantly.[52] The use of a 2.5 nm PVA layer was sufficient to obtain a closed HfO_2 layer after only 50 ALD cycles (≈5 nm). To initiate the HfO_2 ALD growth on the PVA, an ozone pre-treatment was required. As will be discussed in Section 3.3, ozone treatments can also be used to functionalize the graphene directly without the need of a polymer seed-layer, allowing for an even better EOT scaling of the gate dielectric. Despite the potential of polymer seed-layers to obtain uniform ALD growth on graphene without damage, other functionalization approaches offer better opportunities to scale down the dielectric thickness.

3.2. Evaporated Metal and Metal-Oxide Seed-Layers

The relatively low EOT of the polymer buffer layers has led to the exploration of metal and metal-oxide seeding layers to initiate the ALD growth on graphene. The metal and metal-oxide layers can be deposited using e-beam evaporation at room temperature. In the case of using metal seeding-layers these can be oxidized by the exposure of the samples to air after seed-layer deposition[10,60] or by the use of O_2 as a background gas during evaporation.[55] The method was introduced by Kim et al. who used a thin Al seed-layer, oxidized in air during transfer to the ALD chamber, after which 15 nm of Al_2O_3 was deposited by ALD on top.[10] To ensure the Al seed-layer was fully oxidized the sample was exposed to a H_2O step in the ALD chamber at an elevated temperature. FET devices fabricated from the sample showed mobility values up to 8600 $cm^2\ V^{-1}\ s^{-1}$ and a Dirac voltage of 0.08 V, indicating that doping of the graphene can be avoided when a metal seed-layer is used. The dielectric constant of the deposited Al_2O_3 however was relatively low (6.0 instead of 8–9), indicating that further optimization is possible. Despite that the mobility of the graphene devices without the Al_2O_3 seed-layer was not determined, this work shows the potential of using a evaporated metal seed-layer to initiate ALD growth.

The deposition of an Al seed-layer might still damage the graphene despite the good mobility values reported by Kim et al.[10] For example, Fallahazad et al. used an Al seed-layer to initialize the ALD growth of HfO_2 on mono and bi-layer graphene.[60] A strong decrease in the mobility of the graphene was observed after Al evaporation and the deposition of the first 2–4 nm of oxide, as shown in **Figure 9**. The decrease of the mobility was attributed to charged impurities being introduced after seed-layer and dielectric deposition. These were most likely oxygen vacancies present in the deposited Al or HfO_2 films a result of the incomplete oxidation of these layers.

Later work by Fallahazad et al. showed that the Al seed-layer on graphene is also relatively rough when compared to using an Ti seed-layer. This is caused by a higher surface mobility of Al atoms on graphene. The low surface mobility of Ti atoms allowed for the deposition of seed-layers down to 0.6 nm in thickness compared to 2.6 nm for Al. Furthermore the oxidized

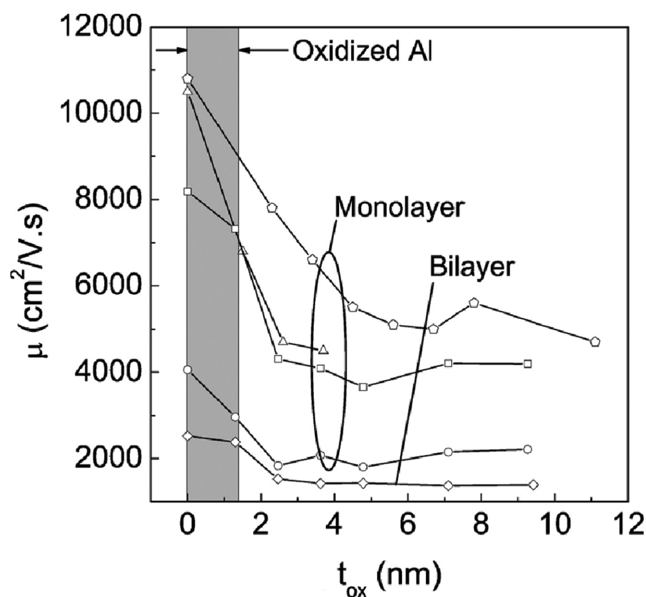

Figure 9. Mobility μ plotted versus the oxide thickness t_{ox} for monolayer and bilayer graphene devices prepared using a e-beam evaporated Al seed-layer and an ALD HfO_2 film. A sharp mobility decrease can be observed for the deposition of the first 2–4 nm of oxide, which remains approximately constant for thicker dielectric films. Adapted with permission.[60] Copyright 2010, AIP Publishing.

© 2017 WILEY-VCH Verlag GmbH & Co. KGaA, Weinheim

Ti seed-layers had a higher dielectric constant 12.7 versus 5.5, making further downscaling of the EOT possible.

Robinson et al. deposited several materials (Al_2O_3, HfO_2, Ta_2O_5 and TiO_2) by ALD on epitaxial graphene. The evaporated metal counterpart of the oxide was used as a seed-layer.[38] Full oxidation of the metal seed-layer was ensured by pulsing H_2O (10 pulses 10 s each) before deposition of the ALD layer. A uniform ALD film could be obtained for all oxides although the ALD deposition temperature strongly affected the coverage. For example Al_2O_3 deposited at 150 °C was rough and contained pin holes, whereas depositing Al_2O_3 at 300 °C led to the deposition of a more uniform film. In the case of Ta_2O_5 closed layers could be obtained, but the resulting films were very rough independent of the deposition temperature. Raman measurements indicated that the deposition of a Ta seed-layer also led to damage to the graphene film, which was in agreement with a strong reduction of the carrier mobility observed by the hall measurements. The use of an Al seed-layer resulted in a reduction of the mobility similar in magnitude as observed by Fallahazad and Farmer et al.[49,60] For HfO_2 a slight increase in the mobility of graphene was observed after ALD and a significant increase for TiO_2. The increase observed after deposition of a Ti seed-layer and subsequent ALD is possibly caused by the charge compensation of the substrate induced doping, often observed for SiC substrates. This observation was supported by an approximately twofold decrease in the charge carrier concentration of graphene after ALD.

The use of metal-oxide seed-layers to initiate the ALD growth on graphene was investigated first by Hsu et al. who e-beam evaporated 5 nm of SiO_2 on graphene followed by ALD of 15 nm of Al_2O_3 for the fabrication of RF transistors.[61] The mobility of the fabricated devices reduced from 2000 ± 500 $cm^2\ V^{-1}\ s^{-1}$ before dielectric deposition to ≈500 $cm^2\ V^{-1}\ s^{-1}$ after e-beam evaporation and ALD, the SiO_2 seed-layer being the most likely cause for the significant degradation of the graphene. Such a significant degradation of the carrier mobility after SiO_2 e-beam evaporation was also observed by Hollander et al. who used it to initiate the ALD growth of HfO_2 on graphene, as illustrated in **Figure 10**. Part of the mobility reduction could be due to the relatively low dielectric constant of the SiO_2 seed-layer, which is known to enhance the impurity scattering in the graphene.[96]

Beside SiO_2 seed-layers also Al_2O_3 and HfO_2 seed-layers were investigated by Hollander et al. Both the Al_2O_3 and HfO_2 seed-layers, ≈2 nm thick, showed an improvement of the mobility irrespective of whether Al_2O_3 or HfO_2 was deposited on the seed-layers. Raman spectroscopy confirmed that the graphene was indeed not damaged by the seed-layer deposition. The use of a HfO_2 seed-layer increased the mobility further compared to Al_2O_3 (see Figure 10). This is a result of the higher dielectric constant of HfO_2, which helps to reduce the charged impurity scattering through dielectric screening.[97] Although both the heterogeneous material stack (Al_2O_3/HfO_2 or HfO_2/Al_2O_3) and homogeneous stacks (Al_2O_3/Al_2O_3 or HfO_2/HfO_2) improved the graphene properties, the dielectric performance of the homogenous material stacks was superior to the heterogeneous stacks. The larger roughness of the heterogeneous stacks combined with the trapping of charges at the interface between the two different dielectrics being the most likely cause for the lower performance. Despite the good properties obtained for the homogenous stacks, still a hysteresis of 0.5 to 0.7 V was observed in the measured transfer curves, indicating that even for these devices trapped charges remain present in the deposited oxide layer. These trapped charges limit the improvement of the graphene devices after dielectric deposition.

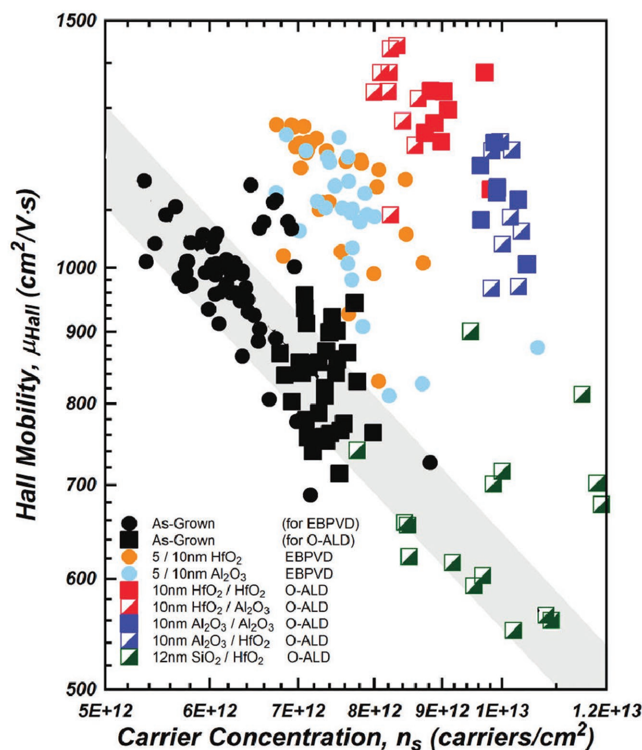

Figure 10. Evaluation of the hall mobility μ_{hall} as a function of the carrier concentration n_s for graphene devices fabricated on SiC. The results indicate that the deposition of a high-κ dielectric on the epitaxial graphene by either oxide seeded ALD (O-ALD) or e-beam evaporation (EBPVD) leads to a mobility improvement. Furthermore, the ALD seeded devices outperform the devices fully prepared by EBPVD. Adapted with permission.[59] Copyright 2011, American Chemical Society.

The quality of both the graphene and the dielectric deposited thus strongly depend on the type of metal or metal-oxide seed-layer deposited by e-beam evaporation. The use of Ti as a seed-layer shows the most promise due to the reduced roughness of the e-beam evaporated films and higher dielectric constant compared to for example Al, Ta and SiO_2 e-beam evaporated films, furthermore the Ti seed-layer did not damage the graphene. Hf seed-layers are also an option, but care should be taken that the deposition temperature of the ALD process is low enough to prevent the formation of Hf-C bonds which disrupt the sp^2 C backbone of graphene and deteriorate its electrical properties, as discussed in Section 2.2.

Apart from e-beam evaporated metal or metal-oxide seed-layers almost no other deposition techniques have been investigated to achieve uniform ALD nucleation. This is because other PVD techniques easily damage the graphene.[13] Jeong et al. for example tried to use sputtered ZnO as a seed-layer to achieve uniform HfO_2 growth on graphene.[51] Although uniform HfO_2 layers of ≈17 nm could be deposited on the sputtered ZnO, Raman analysis showed that the graphene was completely

 © 2017 WILEY-VCH Verlag GmbH & Co. KGaA, Weinheim

etched after the ZnO deposition, due to sputtering induced plasma damage. Since this plasma damage is intrinsic to the sputtering technique, it is not suited for the deposition of ALD nucleation layers on graphene.

Consequently, the combination of PVD techniques, such as e-beam evaporation, sputtering or pulsed laser deposition with ALD to obtain uniform dielectric layers on graphene is a compromise. On one side the material quality and thickness control of ALD is superior to those of the PVD techniques and it prevents damaging the graphene, but the inert nature of the graphene makes nucleation difficult. PVD techniques on the other hand make deposition on the graphene possible but suffer from low material quality, limited thickness control and damage to the graphene.[13] Combining PVD with ALD therefore limits the exposure time of graphene to reactive species, such as ions, which are inherent to PVD techniques, and could damage it significantly. Therefore, completely avoiding this damage remains difficult. The deposition of uniform layers with ALD directly on graphene would avoid these issues, which will be discussed in the next section.

3.3. Surface Functionalization

The use of polymer seed-layers to initialize ALD growth on graphene makes it difficult to achieve good EOT scaling, but avoids damaging the graphene. Metal and metal-oxide seed-layers on the other hand easily damage the graphene, but provide good EOT scaling. To circumvent the tradeoff between these two approaches the direct ALD on graphene using surface functionalization treatments has been investigated extensively in literature, for example by using ozone or O_2 and N_2 plasma treatments. The treatments create oxygen and nitrogen functional groups on the graphene on which the ALD precursor molecules can adsorb, ideally allowing for the deposition of a uniform ALD layer.

The use of O_3 pre-treatments, or the replacement of the H_2O co-reactant by O_3 was investigated first. This is because plasma treatments are generally considered more aggressive and are expected to easily damage the graphene, whereas O_3 treatments are relatively mild. Lee et al. studied the deposition of Al_2O_3 on HOPG, comparing the normal H_2O Al_2O_3 ALD process with a process where the H_2O pulse was replaced by O_3 exposure.[24] For the H_2O based process only ALD growth on the step edges of the HOPG was observed, whereas for the O_3 ALD process a more random nucleation was obtained. However, for both processes no uniform deposition of Al_2O_3 was obtained after 50 ALD cycles at 200 °C. To obtain uniform deposition of Al_2O_3 on the HOPG an additional ozone pretreatment was required. The ozone pretreatment followed by the O_3 ALD process resulted in the deposition of closed Al_2O_3 layers down to 9.5 nm thick. XPS analysis showed that the O_3 pretreatment created epoxide (C−O) carbonyl (C=O) and carboxyl (O−C=O) containing surface groups on the HOPG surface, which enhanced the ALD nucleation but also indicated a change of *sp*^{2} C to *sp*^{3} C which is likely to deteriorate graphene device performance. Similar observations were made by Prikle et al. who showed that an O_3 ALD process increases the nucleation density of the Al_2O_3 on HOPG, but who also found that achieving a closed layer remains difficult when no O_3 pretreatment is used.[65] However, because HOPG is not suited for device fabrication the influence of the O_3 treatment on the properties of the graphene remained unclear.

The importance of the O_3 pretreatment before ALD was investigated further by McDonnel et al. who changed the pulse order during ALD (i.e TMA first or O_3 first) and its effect on the nucleation, see **Figure 11**.[63] First dosing TMA lead to an almost uniformly deposited Al_2O_3 films after 6 ALD cycles. O_3 first however, lead to the selective nucleation of Al_2O_3 growth on the HOPG step edges. XPS measurements of the HOPG surface indicated that short O_3 exposures, as typically used during ALD processing, clean the surface of contaminants and therefore remove possible precursor binding sites. These possible binding sites remain for a TMA first process and thus explain the higher nucleation density compared to the O_3 first

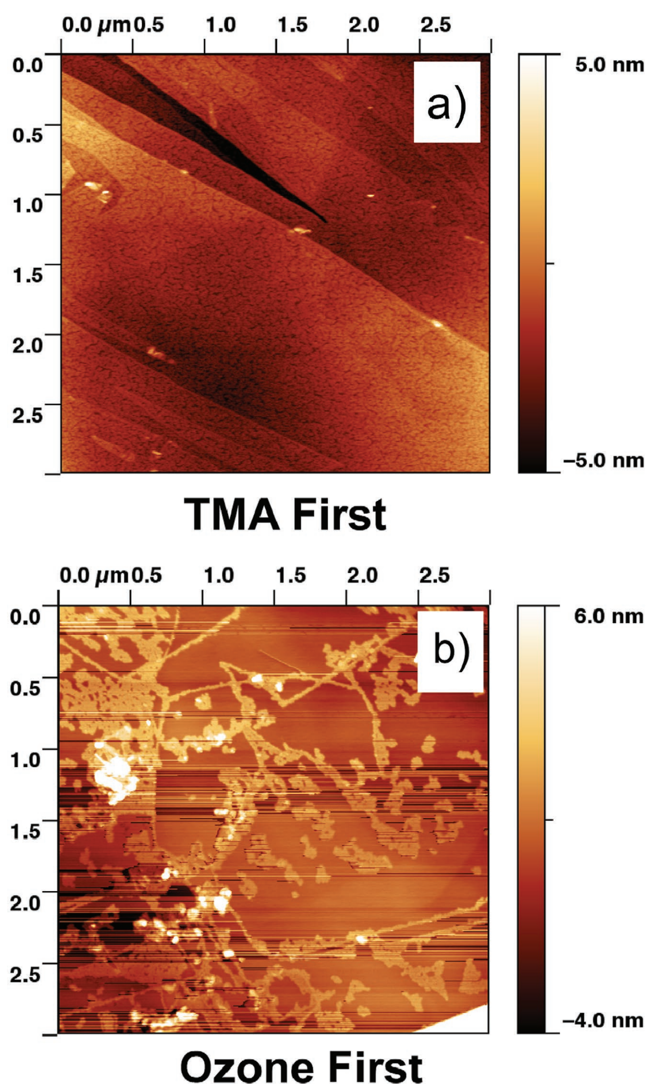

Figure 11. AFM image of Al_2O_3 deposited on HOPG by starting with a) the TMA pulse and b) an O_3 pulse. The difference in coverage illustrates the importance of the ALD pulse sequence on uniformity on ALD Al_2O_3. For the TMA first process an almost uniform layer is obtained whereas for the O_3 first process preferential deposition on the step edges is obtained. Adapted with permission.[63] Copyright 2012, AIP Publishing.

© 2017 WILEY-VCH Verlag GmbH & Co. KGaA, Weinheim

process. Long doses of O_3, like the pretreatments used by Lee et al., first clean the graphene and subsequently create functional groups on the graphene surface.[24,63] The duration of the O_3 pretreatment therefore plays an important role in tuning the nucleation density.

When similar work was done on CVD and exfoliated graphene it was discovered that the O_3 pretreatments at high temperatures (>150 °C) severely damaged the graphene.[66,67] Which agrees with the change from *sp*^{2} C to *sp*^{3} C observed by XPS, discussed above. Lee et al. however showed that at low temperatures (25 °C) damage to the graphene can be prevented. This was later confirmed by Jandhyala et al. who showed, using ab inito calculations, that at temperatures >150 °C the O_3 chemisorbs on the graphene changing the *sp*^{2} carbon backbone to *sp*^{3} carbon.[67] At 25 °C however the O_3 physisorbed on the graphene, leaving the *sp*^{2} backbone intact. During the subsequent TMA pulse the physisorbed O_3 reacted with the TMA forming a Al_2O_3 nucleation layer. The quality of the Al_2O_3 deposited at 25 °C is however, not optimal. To improve this the temperature was increased after 4 TMA/H_2O cycles at 25 °C to 150 °C where an additional 32 cycles of TMA/ H_2O ALD were performed, obtaining a uniform Al_2O_3 layer of 4.5 nm thick. Fabricated FETs showed an significant increase of the mobility after Al_2O_3 deposition with a maximum of ≈19.000 cm^2 V^{-1} s^{-1}. The increase in the mobility was attributed to the removal of surface contaminants by the ozone treatments, such as resist residues left over from the graphene transfer process, the barrier properties of the Al_2O_3 preventing impurities, such as O_2 and H_2O, adsorbing on the graphene and the charge screening of the Al_2O_3 dielectric.

A combination of O_3 ALD and the substrate enhanced nucleation of Ni (Section 2.5) was used by Martin et al. to deposit Al_2O_3 layers on graphene for the integration of graphene in a spin selective membrane in magnetic tunnel junctions (MTJ). A closed layer was obtained after only 6 ALD cycles, corresponding to a thickness of 0.6 nm. These are the thinnest uniform Al_2O_3 layers on graphene reported to date. The ALD layers are thinner than any of the polymer, metal or metal-oxide seed-layers discussed in Sections 3.1 and 3.2. Despite that not always a metal substrate can be used to enhance nucleation, this shows the promise of O_3 functionalization to deposit ultrathin dielectrics on graphene.

Apart from O_3 functionalization also NO_2 has been extensively investigated in literature as a replacement for the H_2O step in the ALD process. The method was introduced by Farmer et al. for the deposition of Al_2O_3 on single wall carbon nanotubes,[98] and later adapted for the nucleation of Al_2O_3 on graphene by Williams et al. who used 50 NO_2/TMA ALD cycles at room temperature followed by 305 cycles of H_2O/TMA at 225 °C to deposit ≈30 nm thick continuous Al_2O_3 films on graphene.[71] The NO_2 adsorbs non-covalently on the graphene surface, most likely through a charge transfer mechanism.[69] In the subsequent TMA exposure the NO_2 reacts with the TMA forming Al_2O_3 islands. Because the NO_2 does not adsorb on Al_2O_3 the reaction stops when the entire graphene surface is covered by Al_2O_3, at a thickness of ≈8.0 nm. The relatively large thickness required before growth stops, could indicate that even with NO_2 the nucleation on graphene is not completely uniform. Later work by Farmer et al. showed that the use of NO_2 as a reactant gas instead of H_2O lead to a strong mobility decrease of the graphene.[49] This was later confirmed by Lin et al. who attributed the mobility decrease to the charged impurity scattering of the NO_2 grown Al_2O_3 nucleation layer. The severe deterioration of the graphene's electrical properties, make NO_2 treatments to initialize ALD growth unsuited for device applications. Other applications however, where the quality of the graphene is not important, NO_2 functionalization can still be used. An example is the fabrication of thin oxide membranes. In this case the graphene is only used as a growth support and etched after ALD processing, which makes it possible to fabricate of 2.8 nm thick freestanding Al_2O_3 membranes.[72]

Wheeler et al. investigated the exposure of graphene to XeF_2 gas to enhance ALD of Al_2O_3 on graphene.[81] Graphene was exposed to XeF_2 for various exposure times. The XeF_2 dissociates on the graphene at room temperature forming C—F functional groups. The amount of C—F groups created increased as a function of the XeF_2 exposure time. An optimum was found for a C—F group coverage of approximately 6–7%, where a uniform Al_2O_3 layer was deposited on the graphene after ≈15 nm. Lower coverages did not result in a closed graphene layer, higher coverages of C—F could not be obtained due to the formation of CF_2 which decreased the total density of reactive surface sites. Hall measurements showed a ≈10–15% increase in the mobility after Al_2O_3 ALD. This mobility increase is smaller than normally observed after Al_2O_3 ALD,[59,67] possibly due to charged impurity scattering at the graphene/Al_2O_3 interface.

The use of plasma treatments to obtain the uniform nucleation of ALD on graphene was first reported by Nayfeh et al. who replaced the H_2O co-reactant dose by a O_2 plasma step, for the deposition of Al_2O_3 on graphene.[74] Fabricated devices containing the plasma deposited Al_2O_3 as a gate dielectric were compared to devices with a SiO_2 e-beam evaporated dielectric. The plasma prepared Al_2O_3 devices performed significantly better, but this is most likely due to the poor quality of the SiO_2 devices (as discussed in Section 3.2). Furthermore the dielectric constant of SiO_2 is significantly lower compared to that of Al_2O_3, which could also explain the difference in performance. Raman measurements of both the plasma deposited Al_2O_3 and the SiO_2 e-beam reference samples revealed defects, indicating that the graphene is indeed damaged by the O_2 plasma. Later work by Lim et al. showed that N_2 plasma pre-treatments can also be used for the uniform deposition of Al_2O_3 on graphene.[73] It was suggested that the N_2 plasma creates defects in the graphene, which act as nucleation sites for the TMA or H_2O precursor and co-reactant. The nature of the defects sites created was not investigated, but these are most likely nitrogen containing surface groups, which react with the TMA, similarly as observed for the NO_2/TMA process.

To circumvent the damaging of the graphene by an O_2 plasma treatment Shin et al. performed the O_2 plasma treatment on a sacrificial graphene layer.[39] The O_2 plasma treatment created epoxide and carboxyl groups on the graphene, converting it to graphene oxide (GO). This GO was transferred on top of an untreated graphene layer. Next 22.3 nm of Al_2O_3 was deposited on the graphene /GO stack. The deposition of a smooth and continuous Al_2O_3 film, was confirmed by Atomic force microscopy (AFM). Nourbakhsh et al. also performed O_2

© 2017 WILEY-VCH Verlag GmbH & Co. KGaA, Weinheim

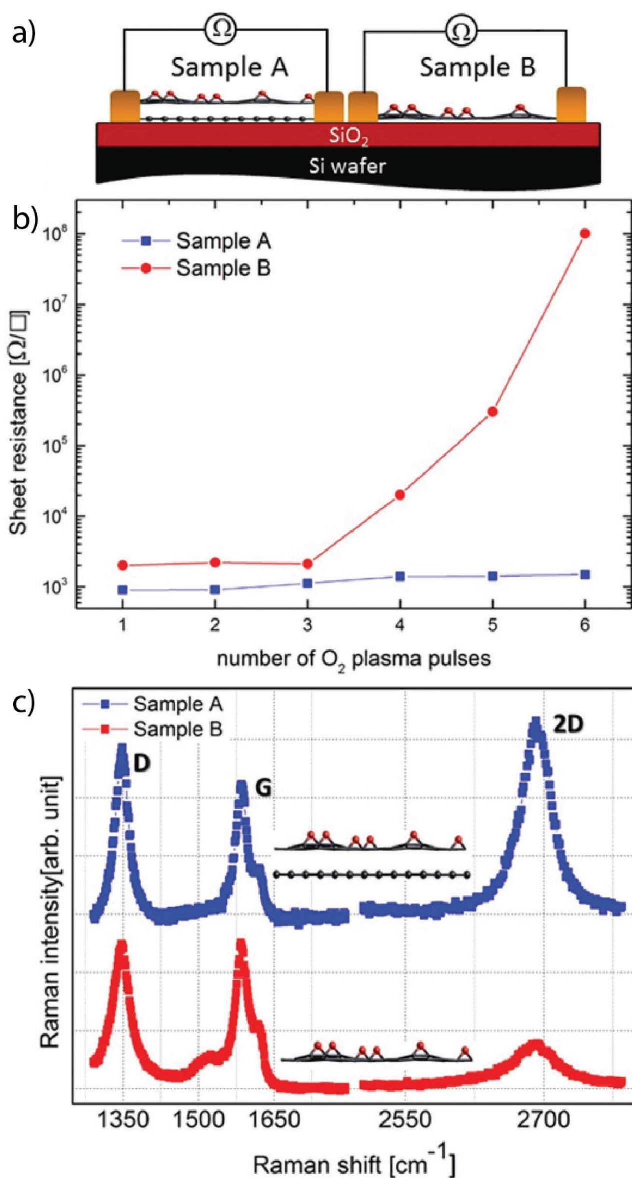

Figure 12. a) Schematic diagram of the method employed by Nourbakhsh et al. For sample A the underlying graphene is protected by a sacrificial graphene layer. An unprotected graphene layer is used as a reference, sample B. b) Relationship between the sheet resistance and the number of O_2 plasma pulses for the protected and unprotected sample. c) Raman spectra of the protected and unprotected sample after 6 O_2 plasma pulses. Adapted with permission.[77] Copyright 2015, The Royal Society of Chemistry.

plasma treatments on a sacrificial graphene layer which was, transferred on top of the graphene channel before the plasma treatment, as illustrated in **Figure 12**.[77] The top layer of graphene was oxidized by the O_2 plasma exposure and at the same time protected the underlying graphene layer. With this method uniform Al_2O_3 layers down to 4 nm could be deposited. FET devices fabricated with the abovementioned processes preformed similarly to back-gated graphene-FETs and showed an improved gate capacitance over Al e-beam seeded Al_2O_3 FETs.[77,78] A disadvantage of using a sacrificial graphene layer is the requirement of an additional graphene transfer step. This makes the functionalization process time consuming. Furthermore, the extra transfer step, could trap polymer residues left over from the previous transfer procedure in between the graphene layers. To avoid the need for an additional transfer step Nath et al. spin-coated GO flakes prepared by chemical exfoliation on top of epitaxial graphene.[79] The GO layer (≈1.5 nm thick) acted as a seed-layer for the subsequent ALD growth of Al_2O_3, HfO_2 and TiO_2. The GO was stable up to 400 °C, which made it possible to deposit the films at the optimal ALD process conditions, without damaging the epitaxial graphene. The dielectric constants of the deposited films were identical to those deposited on a Si witness sample and close to their ideal values.[79]

Vervuurt et al. developed a plasma functionalization method which avoids the use of a sacrificial graphene or GO layer altogether.[32] In this case the graphene was functionalized by a H_2 plasma treatment. The H_2 plasma treatment created C—H functional groups on the graphene surface, enhancing the adsorption of the TMA precursor molecules, allowing for the deposition of uniform Al_2O_3 films down to 8 nm in thickness on graphene. As for O_2 plasma treatments, the H_2 plasma treatment initially led to the sp^3 hybridization of graphene, which resulted in a drastic reduction of the graphene charge carrier mobility. Contrary to O_2 plasma functionalized graphene however, this reduction in charge carrier mobility was fully recovered upon Al_2O_3 ALD. Subsequent annealing at 400 °C further improved the mobility. Density functional theory calculations showed that this is caused by the abstraction of hydrogen functional groups from the graphene upon Al_2O_3 precursor adsorption, which recovered the sp^2 hybridization of the graphene (see **Figure 13**).

Johns et al. replaced the H_2O pulse with atomic oxygen, created by flowing O_2 along a heated tungsten filament, for the growth of ZnO on epitaxial graphene.[80] The exposure of graphene to atomic oxygen led to the formation of epoxide groups on the graphene surface. The subsequent exposure to the diethyl zinc precursor (DEZ) abstracted these oxygen groups from the graphene surface, creating mobile metal oxide clusters no longer bonded to the graphene.[99] AFM images showed the uniform nucleation of ZnO on the graphene, while Raman analysis indicated that no defects where created in the graphene after the atomic oxygen and DEZ exposure. No closed layers were grown however, probably because the atomic oxygen exposure and DEZ exposure were performed at room temperature, whereas for the removal of reaction products and other physisorbed species the sample needed to be heated to 200 °C at the end of each ALD cycle, making the process time consuming.

The use of different surface functionalization techniques, such as O_3, NO_2 and plasma treatments, make it possible to deposit uniform dielectric layers by ALD on graphene without the need for thick nucleation layers. When the treatments are performed at a sufficiently low temperature, the reaction with the sp^2 basal plane of graphene can be avoided and the deterioration of the graphene's electrical properties can be minimized or prevented all together. The downside is that the low deposition temperatures, generally lead to dielectrics of lower quality being deposited. Performing a few cycles at low temperature to

 © 2017 WILEY-VCH Verlag GmbH & Co. KGaA, Weinheim

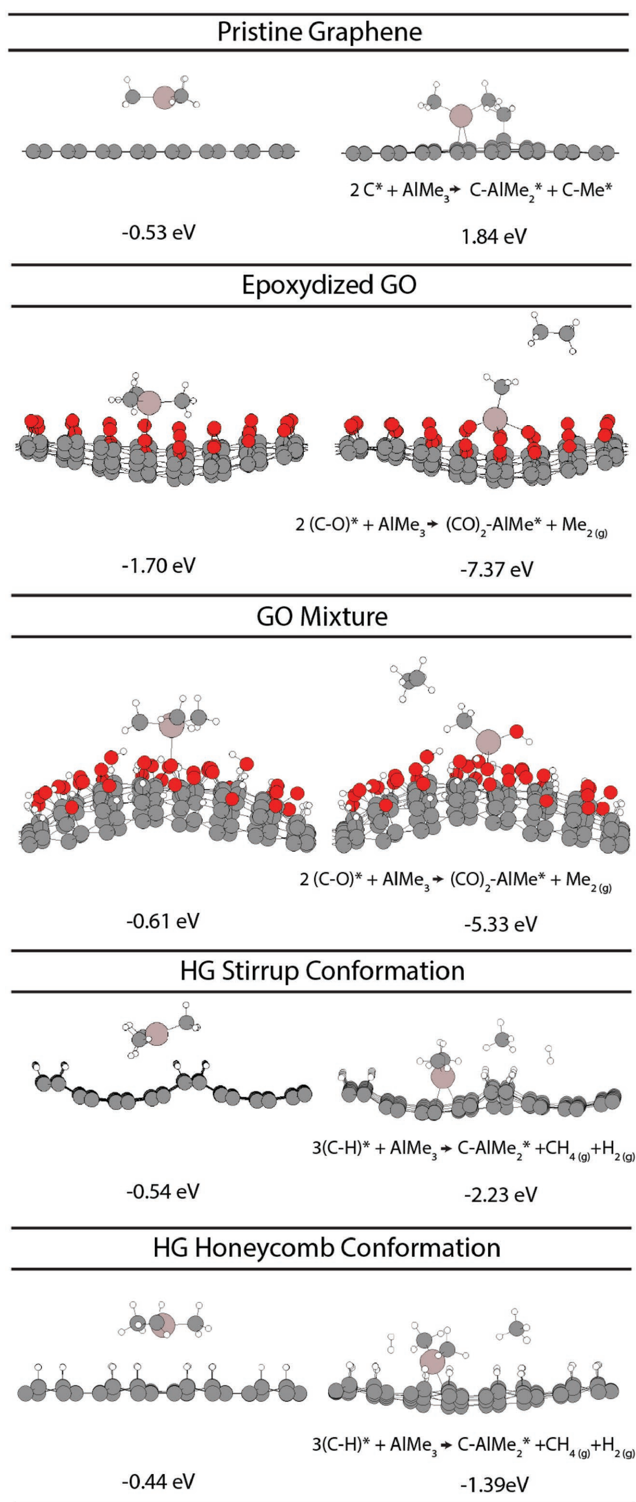

Figure 13. DFT-predicted structures and related relative energies of the lowest-energy (left) physisorbed and (right) chemisorbed species on pristine graphene, oxygenated graphene (i.e. graphene oxide, GO) and hydrogenated graphene (HG). For GO and HG the two most likely configurations are given. The adsorption of TMA on hydrogenated graphene is accompanied by the release of H_2 from the graphene surface, restoring the graphene to its pristine sp^2 C state. Adapted with permission.[32] Copyright 2017, American Chemical Society.

initialize the nucleation on the graphene followed by depositing the remaining material at higher temperatures is an option, but also makes the process time consuming due to the need to cool-down and heat the ALD system between two deposition runs. The need for a low processing temperature can be avoided by the use of a sacrificial functionalized graphene layer, such as GO.[79] Additionally certain precursor chemistries or functionalization methods recover the pristine graphene sp^2 hybridization during ALD, making it possible to directly deposit materials on graphene at elevated temperatures without damage.[32] Moreover, when compared with other graphene surface preparation methods, the surface functionalization techniques have the advantage that they can be done in the same system without breaking the vacuum as is the case for most other deposited seed-layers. This could help to improve the quality of the seed-layer/dielectric interface, since the contamination of the samples with adventitious carbon, due to the exposure to air, is avoided.

3.4. Wet Chemistry

Apart from the dry functionalization approaches discussed in the previous section, also wet chemical functionalization has been explored to obtain uniform ALD growth on graphene. Cao et al. soaked the graphene in H_2O for approximately 4 h before Al_2O_3 ALD growth. It was found that the Al_2O_3 was uniformly deposited on the graphene, a result attributed to the presence of physisorbed water at the graphene surface. The Al_2O_3 was deposited at a temperature of 200 °C, well above the desorption temperature of H_2O. This would suggest that if the Al_2O_3 deposition is not started quickly the H_2O will desorb from the graphene, which will result in the deposition of discontinuous ALD films. A similar approach has been used by Zheng et al. who exposed the graphene to several H_2O pulses before starting the ALD process at 100 °C.[82] Uniform Al_2O_3 deposition was obtained after ≈4 nm of Al_2O_3 deposition. Despite the dependence of H_2O pre-treatments on deposition temperature and dwell-time it might have some advantages over, for example, O_3 functionalization. Work by Webber et al. indicated that the amount of trapped charges in Al_2O_3 deposited by ALD is reduced for H_2O pretreatments combined with the thermal ALD of Al_2O_3 compared to the O_3 based ALD process.[68] The better performance of the thermal process was attributed to the higher deposition temperature (120 °C vs. 80 °C) leading to a more dense film being deposited. Furthermore Al_2O_3 prepared using O_3 is known to be oxygen rich, due to the incorporation of carbonate groups from incomplete surface reactions. These can possibly act as charge traps.

Garces et al. investigated the use of cleaning epitaxial graphene in a HF and/or NH_4OH:H_2O_2 solution to achieve a higher nucleation density of Al_2O_3 on graphene.[85] The HF solution was intended to remove any possible oxides and other impurities from the graphene surface. While the NH_4OH:H_2O_2 treatment created hydroxyl terminated functional groups on the graphene as confirmed by XPS. The combination of the two treatments led to the uniform deposition of ≈30 nm Al_2O_3. Hall mobility measurements showed no change in mobility after functionalization and ALD. The dielectric constant of the Al_2O_3

© 2017 WILEY-VCH Verlag GmbH & Co. KGaA, Weinheim

was confirmed to be 7.6, which is lower than on the Si witness samples for which a dielectric constant of 9 was measured. The lower dielectric constant obtained for the Al_2O_3 deposited on graphene was attributed to possible hydroxide and carbide impurities trapped in the film.

The number of wet chemistry approaches investigated to functionalize graphene is limited. Part of this is because the created reactive species on the graphene are physisorbed rather than chemisorbed. Chemisorbed species are more stable but also disrupt the graphene sp^2 configuration, deteriorating its electronic properties. For this reason most wet chemical based approaches rely on increasing the amount of physisorbed species. This makes these methods such as H_2O soaking and H_2O pulsing heavily dependent on the time until ALD is performed and the substrate temperature used during the ALD process. The reproducibility is therefore an important issue, for these functionalization methods. However, in the available literature this is rarely discussed. Furthermore, in the case of CVD graphene the adhesion to the underlying substrate is not very good. Submerging graphene in H_2O can therefore lead to the delamination of the graphene from the substrate due to the intercalation of H_2O. The simplicity of the H_2O treatment methods might still be a viable alternative, but the reproducibility of the method needs further investigation.

4. Summary and Outlook

The integration of graphene in optical and electronic devices, often requires the deposition of high-k dielectrics on graphene. ALD is the method of choice due to its precise thickness control, low deposition temperature and ability to deposit high quality materials uniformly over a large area. The direct ALD on graphene typically results in selective growth on grain boundaries wrinkles and defect sites, caused by a lack of reactive surface sites on graphene's basal plane on which precursors molecules can adsorb. ALD precursor molecules tend to physisorb on graphene instead of forming a chemical bond. The graphene cleanliness and ALD process conditions such as substrate temperature, pump times, purge times and the precursor chemistry strongly affect the deposition uniformity. The appropriate choice of precursor, dose and purge times as well as a low deposition temperature and suitable underlying substrate (e.g. Cu) can increase the ALD nucleation on pristine graphene. However for many applications the substrate material is a given, and the choice of precursors molecules is often limited. Decreasing the substrate temperature likely also decreases the quality of the material being deposited and thus a tradeoff must be made. Furthermore, the strong dependence on process conditions might affect process reproducibility. To avoid making this compromise and increase process reproducibility seed-layers or surface functionalization can be used for ALD of uniform films on graphene.

Polymer, metal and metal-oxide seed-layers make it possible to deposit uniform films by ALD on graphene. Polymer buffer layers avoid damage to the graphene but can unintentionally dope it, shifting the charge neutrality point far beyond realistic device operating regimes. Furthermore the low dielectric constant of the polymers used and relative high thickness of the polymer/dielectric stack make dielectric scaling difficult. The deposition of metal and metal-oxide seed-layers often deteriorate graphene's electrical properties due to deposition induced damage. In addition scattering of charge carriers in the graphene can be increased due to the incomplete oxidation of the metal seed-layer, leading to a decrease in charge carrier mobility.

The use of surface functionalization techniques makes it possible to deposit uniform dielectrics on graphene by ALD. The functional groups act as ALD precursor adsorption sites, increasing the deposition uniformity. The creation of these groups, can lead to the conversion of sp^2 carbon bonds to sp^3 carbon, disrupting the graphene basal plane and deteriorating its properties. However, when the functionalization temperature is sufficiently low, the disruption of the sp^2 carbon bonds of the graphene can be avoided because the functionalization proceeds via physisorption instead of chemisorption. This means that the ALD temperature needs to be kept low as well to avoid the desorption of the physisorbed functional groups. The lower deposition temperature conversely results in dielectrics of lower quality being deposited. Increasing the deposition temperature after the first few cycles is an option, but makes the process elaborate. Similarly, the wet chemistry functionalization approaches enhance the ALD nucleation by increasing the amount of physisorbed species on the graphene. Physisorbed species are however less stable on the graphene surface compared to chemisorbed ones. Reproducibility can therefore be an issue.

The use of a sacrificial graphene layer that protects the underlying graphene during functionalization might also be an option. In this case the conversion of sp^2 to sp^3 bonds only takes place on the top layer and ALD can be performed at higher temperatures. Reversible H_2 plasma functionalization provides a satisfactory compromise in which the graphene is functionalized directly but the sp^2 hybridization of graphene is recovered after ALD due to the abstraction of the functional groups during the ALD process.

The overview given in this review indicates that there are many possibilities to grow dielectrics on graphene by ALD uniformly, each methods having its advantages and disadvantages. In the ideal case one would like to have a method that enables direct uniform ALD growth on graphene without damage to the graphene at a sufficiently high temperature to produce a high quality dielectric. The functionalization of graphene by a reversible plasma treatment or the like and/or increasing the ALD precursor dose times offer the best opportunities from an experimental point of view. These are relatively easy to implement and many ALD systems are equipped with a plasma source. The use of a sacrificial layer also works well but is relatively time consuming due to the additional graphene transfer step. In all three cases the functionalization and further ALD processing can be done in the same system at a constant temperature, without the need for additional equipment or breaking the vacuum in-between functionalization and dielectric deposition.

Apart from the deposition of high-k dielectric materials by ALD, the uniform deposition of metals on graphene is also of interest, for example for the fabrication of metal-graphene contacts by ALD. In this case the damage to the graphene observed for plasma functionalization or other functionalization methods to initialize the growth might be beneficial. It

© 2017 WILEY-VCH Verlag GmbH & Co. KGaA, Weinheim

has been shown for evaporated contacts that plasma treatments can improve the metal-graphene interaction.[100–102] So both uniform ALD nucleation and a better metal-graphene contact might be achievable when combining plasma functionalization with metal ALD. Recently, Thissen et al. have shown that using an e-beam induced deposited (EBID) seed-layer of Pt, A film of Pt can be grown uniformly on graphene. Fabricated devices with EBID-ALD deposited contacts showed high quality Pt-graphene contacts, likely due to the improved Pt-graphene interaction achieved by the EBID Pt seed-layer.[103] Despite the significant advances in ALD materials on graphene over the past few years further improvements and innovations are still required. Especially increasing the dielectric layer quality while maintaining uniform ALD growth will prove essential to the further improvement of device performance and the reduction of EOT. A better understanding of the chemistry behind the functionalization and subsequent ALD process will be vital to achieve this.

Acknowledgements

This work is part of the research program (Projektruimte: 12PR3101) of the Foundation for Fundamental Research on Matter (FOM), which is part of the Netherlands Organization for Scientific Research (NWO).

Conflict of Interest

The authors declare no conflict of interest.

Keywords

atomic layer deposition, dielectrics, functionalization, graphene

Received: February 23, 2017
Revised: April 12, 2017
Published online: May 26, 2017

[1] A. K. Geim, K. S. Novoselov, *Nat. Mater.* **2007**, *6*, 183.
[2] F. Xia, D. B. Farmer, Y. Lin, P. Avouris, *Nano Lett.* **2010**, *10*, 715.
[3] F. Schwierz, *Nat. Nanotechnol.* **2010**, *5*, 487.
[4] W. F. Smith, J. Hashemi, *Foundations of Materials Science and Engineering*, McGraw-Hill, Boston, USA, **2005**.
[5] W. Cheol Shin, T. Yong Kim, O. Sul, B. Jin Cho, *Appl. Phys. Lett.* **2012**, *101*, 33507.
[6] V. K. Sangwan, D. Jariwala, S. A. Filippone, H. J. Karmel, J. E. Johns, J. M. P. Alaboson, T. J. Marks, L. J. Lauhon, M. C. Hersam, *Nano Lett.* **2013**, *13*, 1162.
[7] M. Popinciuc, C. Józsa, P. J. Zomer, N. Tombros, A. Veligura, H. T. Jonkman, B. J. van Wees, *Phys. Rev. B* **2009**, *80*, 214427.
[8] M.-B. Martin, B. Dlubak, R. S. Weatherup, H. Yang, C. Deranlot, K. Bouzehouane, F. Petroff, A. Anane, S. Hofmann, J. Robertson, A. Fert, P. Seneor, *ACS Nano* **2014**, *8*, 7890.
[9] S. Banerjee, L. Register, E. Tutuc, D. Reddy, A. H. MacDonald, *IEEE Electron Device Lett.* **2009**, *30*, 158.
[10] S. Kim, J. Nah, I. Jo, D. Shahrjerdi, L. Colombo, Z. Yao, E. Tutuc, S. K. Banerjee, *Appl. Phys. Lett.* **2009**, *94*, 62107.
[11] M. C. Lemme, L. Li, T. Palacios, F. Schwierz, *MRS Bull.* **2014**, *39*, 711.
[12] A. Pakkala, M. Putkonen, in *Handb. Depos. Technol. Film. Coatings*, Elsevier, **2010**, pp. 364–391.
[13] Z. H. Ni, H. M. Wang, Y. Ma, J. Kasim, Y. H. Wu, Z. X. Shen, *ACS Nano* **2008**, *2*, 1033.
[14] X. Wang, S. M. Tabakman, H. Dai, *J. Am. Chem. Soc.* **2008**, *130*, 8152.
[15] K. Kim, H.-B.-R. Lee, R. W. Johnson, J. T. Tanskanen, N. Liu, M.-G. Kim, C. Pang, C. Ahn, S. F. Bent, Z. Bao, *Nat. Commun.* **2014**, *5*, 4781.
[16] B. Karasulu, R. H. J. Vervuurt, W. M. M. Kessels, A. A. Bol, *Nanoscale* **2016**, *8*, 19829.
[17] L. Liao, X. Duan, *Mater. Sci. Eng. R: Reports* **2010**, *70*, 354.
[18] N. Y. Garces, V. D. Wheeler, D. K. Gaskill, *J. Vac. Sci. Technol. B Microelectron. Nanom. Struct.* **2012**, *30*, 30801.
[19] J. Kim, S. Jandhyala, *Thin Solid Films* **2013**, *546*, 85.
[20] C. Marichy, N. Pinna, *Coord. Chem. Rev.* **2013**, *257*, 3232.
[21] I.-K. Oh, J. Tanskanen, H. Jung, K. Kim, M. J. Lee, Z. Lee, S.-K. Lee, J.-H. Ahn, C. W. Lee, K. Kim, H. Kim, H.-B.-R. Lee, *Chem. Mater.* **2015**, *27*, 5868.
[22] A. I. Aria, K. Nakanishi, L. Xiao, P. Braeuninger-Weimer, A. A. Sagade, J. A. Alexander-Webber, S. Hofmann, *ACS Appl. Mater. Interfaces* **2016**, *8*, 30564.
[23] Y. Xuan, Y. Q. Wu, T. Shen, M. Qi, M. A. Capano, J. A. Cooper, P. D. Ye, *Appl. Phys. Lett.* **2008**, *92*, 13101.
[24] B. Lee, S. Park, H.-C. Kim, K. Cho, E. M. Vogel, M. J. Kim, R. M. Wallace, J. Kim, *Appl. Phys. Lett.* **2008**, *92*, 203102.
[25] F. Speck, M. Ostler, J. Röhrl, K. V. Emtsev, M. Hundhausen, L. Ley, T. Seyller, *Phys. Status Solidi* **2010**, *7*, 398.
[26] B. Dlubak, P. R. Kidambi, R. S. Weatherup, S. Hofmann, J. Robertson, *Appl. Phys. Lett.* **2012**, *100*, 173113.
[27] R. S. Edwards, K. S. Coleman, *Nanoscale* **2013**, *5*, 38.
[28] X. Li, X. Meng, J. Liu, D. Geng, Y. Zhang, M. N. Banis, Y. Li, J. Yang, R. Li, X. Sun, M. Cai, M. W. Verbrugge, *Adv. Funct. Mater.* **2012**, *22*, 1647.
[29] C. Ban, M. Xie, X. Sun, J. J. Travis, G. Wang, H. Sun, A. C. Dillon, J. Lian, S. M. George, *Nanotechnology* **2013**, *24*, 424002.
[30] M. Yu, A. Wang, Y. Wang, C. Li, G. Shi, *Nanoscale* **2014**, *6*, 11419.
[31] K. S. Novoselov, A. K. Geim, S. V. Morozov, D. Jiang, Y. Zhang, S. V. Dubonos, I. V. Grigorieva, A. A. Firsov, *Science* **2004**, *306*, 666.
[32] R. H. J. Vervuurt, B. Karasulu, M. A. Verheijen, W. (Erwin) M. M. Kessels, A. A. Bol, *Chem. Mater.* **2017**, *29*, 2090.
[33] Y.-Q. Cao, Z.-Y. Cao, X. Li, D. Wu, A.-D. Li, *Appl. Surf. Sci.* **2014**, *291*, 78.
[34] D. Van Lam, S.-M. Kim, Y. Cho, J.-H. Kim, H.-J. Lee, J.-M. Yang, S.-M. Lee, *Nanoscale* **2014**, *6*, 5639.
[35] J. Kim, S. Kim, W. Jung, *Mater. Lett.* **2016**, *165*, 45.
[36] K. Zou, X. Hong, D. Keefer, J. Zhu, *Phys. Rev. Lett.* **2010**, *105*, 126601.
[37] I. Meric, M. Y. Han, A. F. Young, B. Ozyilmaz, P. Kim, K. L. Shepard, *Nat. Nanotechnol.* **2008**, *3*, 654.
[38] J. A. Robinson, M. LaBella, K. A. Trumbull, X. Weng, R. Cavelero, T. Daniels, Z. Hughes, M. Hollander, M. Fanton, D. Snyder, *ACS Nano* **2010**, *4*, 2667.
[39] K. S. Park, S. Kim, H. Kim, D. Kwon, Y.-E. Koo Lee, S.-W. Min, S. Im, H. J. Choi, S. Lim, H. Shin, S. M. Koo, M. M. Sung, *Nanoscale* **2015**, *7*, 17702.
[40] A. Tamm, J. Kozlova, L. Aarik, A. Aidla, J. Lu, A. A. Kiisler, A. Kasikov, P. Ritslaid, H. Mandar, L. Hultman, V. Sammelselg, K. Kukli, J. Aarik, *Phys. Status Solidi A* **2014**, *211*, 397.
[41] G. Fisichella, E. Schilirò, S. Di Franco, P. Fiorenza, R. Lo Nigro, F. Roccaforte, S. Ravesi, F. Giannazzo, *ACS Appl. Mater. Interfaces* **2017**, *9*, 7761.
[42] Y. H. Park, M. H. Kim, S. Bin Kim, H. J. Jung, K. Chae, Y. H. Ahn, J.-Y. Park, F. Rotermund, S. W. Lee, *Chem. Mater.* **2016**, *28*, 7268.
[43] R. Liu, M. Peng, H. Zhang, X. Wan, M. Shen, *Mater. Sci. Semicond. Process.* **2016**, *56*, 324.
[44] J. M. P. Alaboson, Q. H. Wang, J. D. Emery, A. L. Lipson, M. J. Bedzyk, J. W. Elam, M. J. Pellin, M. C. Hersam, *ACS Nano* **2011**, *5*, 5223.

 © 2017 WILEY-VCH Verlag GmbH & Co. KGaA, Weinheim

[45] J. Kitzmann, A. Göritz, M. Fraschke, M. Lukosius, C. Wenger, A. Wolff, G. Lupina, *Sci. Rep.* **2016**, *6*, 29223.
[46] K. S. Han, P. Y. Kalode, Y.-E. Koo Lee, H. Kim, L. Lee, M. M. Sung, *Nanoscale* **2016**, *8*, 5000.
[47] J. H. Jeon, S.-K. Jerng, K. Akbar, S.-H. Chun, *ACS Appl. Mater. Interfaces* **2016**, *8*, 29637.
[48] J. H. Park, H. C. P. Movva, E. Chagarov, K. Sardashti, H. Chou, I. Kwak, K.-T. Hu, S. K. Fullerton-Shirey, P. Choudhury, S. K. Banerjee, A. C. Kummel, *Nano Lett.* **2015**, *15*, 6626.
[49] D. B. Farmer, H.-Y. Chiu, Y.-M. Lin, K. A. Jenkins, F. Xia, P. Avouris, *Nano Lett.* **2009**, *9*, 4474.
[50] Y.-M. Lin, C. Dimitrakopoulos, K. A. Jenkins, D. B. Farmer, H.-Y. Chiu, A. Grill, P. Avouris, *Science* **2010**, *327*, 734.
[51] S.-J. Jeong, Y. Gu, J. Heo, J. Yang, C.-S. Lee, M.-H. Lee, Y. Lee, H. Kim, S. Park, S. Hwang, *Sci. Rep.* **2016**, *6*, 20907.
[52] I. Meric, C. R. Dean, A. F. Young, N. Baklitskaya, N. J. Tremblay, C. Nuckolls, P. Kim, K. L. Shepard, *Nano Lett.* **2011**, *11*, 1093.
[53] A. Pirkle, R. M. Wallace, L. Colombo, *Appl. Phys. Lett.* **2009**, *95*, 133106.
[54] D. B. Farmer, Y.-M. Lin, P. Avouris, *Appl. Phys. Lett.* **2010**, *97*, 13103.
[55] B. Fallahazad, K. Lee, G. Lian, S. Kim, C. M. Corbet, D. a. Ferrer, L. Colombo, E. Tutuc, *Appl. Phys. Lett.* **2012**, *100*, 93112.
[56] A. A. Sagade, D. Neumaier, D. Schall, M. Otto, A. Pesquera, A. Centeno, A. Z. Elorza, H. Kurz, *Nanoscale* **2015**, *7*, 3558.
[57] T. Shen, J. J. Gu, M. Xu, Y. Q. Wu, M. L. Bolen, M. A. Capano, L. W. Engel, P. D. Ye, *Appl. Phys. Lett.* **2009**, *95*, 172105.
[58] T. Hopf, K. V. Vassilevski, E. Escobedo-Cousin, P. J. King, N. G. Wright, A. G. O'Neill, A. B. Horsfall, J. P. Goss, G. H. Wells, M. R. C. Hunt, *J. Appl. Phys.* **2014**, *116*, 154504.
[59] M. J. Hollander, M. LaBella, Z. R. Hughes, M. Zhu, K. A. Trumbull, R. Cavalero, D. W. Snyder, X. Wang, E. Hwang, S. Datta, J. A. Robinson, *Nano Lett.* **2011**, *11*, 3601.
[60] B. Fallahazad, S. Kim, L. Colombo, E. Tutuc, *Appl. Phys. Lett.* **2010**, *97*, 123105.
[61] A. Hsu, H. Wang, K. K. Kim, J. Kong, T. Palacios, *Jpn. J. Appl. Phys.* **2011**, *50*, 70114.
[62] B. Lee, G. Mordi, T. Park, L. Goux, Y. J. Chabal, K. Cho, E. M. Vogel, M. Kim, L. Colombo, R. M. Wallace, J. Kim, in *ECS Trans.*, ECS, **2009**, pp. 225–230.
[63] S. McDonnell, A. Pirkle, J. Kim, L. Colombo, R. M. Wallace, *J. Appl. Phys.* **2012**, *112*, 104110.
[64] G. Lee, B. Lee, J. Kim, K. Cho, *J. Phys. Chem. C* **2009**, *113*, 14225.
[65] A. Pirkle, S. McDonnell, B. Lee, J. Kim, L. Colombo, R. M. Wallace, *Appl. Phys. Lett.* **2010**, *97*, 3.
[66] B. Lee, G. Mordi, M. J. Kim, Y. J. Chabal, E. M. Vogel, R. M. Wallace, K. J. Cho, L. Colombo, J. Kim, *Appl. Phys. Lett.* **2010**, *97*, 43107.
[67] S. Jandhyala, G. Mordi, B. Lee, G. Lee, C. Floresca, P.-R. Cha, J. Ahn, R. M. Wallace, Y. J. Chabal, M. J. Kim, L. Colombo, K. Cho, J. Kim, *ACS Nano* **2012**, *6*, 2722.
[68] J. A. Alexander-Webber, A. A. Sagade, A. I. Aria, Z. A. Van Veldhoven, P. Braeuninger-Weimer, R. Wang, A. Cabrero-Vilatela, M.-B. Martin, J. Sui, M. R. Connolly, S. Hofmann, A. Zenas, *2D Mater.* **2016**, *4*, 11008.
[69] M. J. Young, C. B. Musgrave, S. M. George, *ACS Appl. Mater. Interfaces* **2015**, *7*, 12030.
[70] Y.-M. Lin, K. A. Jenkins, A. Valdes-Garcia, J. P. Small, D. B. Farmer, P. Avouris, *Nano Lett.* **2009**, *9*, 422.
[71] J. R. Williams, L. DiCarlo, C. M. Marcus, *Science* **2007**, *317*, 638.
[72] L. Wang, J. J. Travis, A. S. Cavanagh, X. Liu, S. P. Koenig, P. Y. Huang, S. M. George, J. S. Bunch, *Nano Lett.* **2012**, *12*, 3706.
[73] T. Lim, D. Kim, S. Ju, *Appl. Phys. Lett.* **2013**, *103*, 13107.
[74] O. M. Nayfeh, T. Marr, M. Dubey, *IEEE Electron Device Lett.* **2011**, *32*, 473.
[75] X. Tang, N. Reckinger, O. Poncelet, P. Louette, F. Ureña, H. Idrissi, S. Turner, D. Cabosart, J. Colomer, J.-P. Raskin, B. Hackens, L. A. Francis, *Sci. Rep.* **2015**, *5*, 13523.
[76] X. Tang, N. Reckinger, O. Poncelet, P. Louette, J.-F. Colomer, J.-P. Raskin, B. Hackens, L. A. Francis, *arXiv.org, e-Print Arch. Condens. Matter* **2014**, 1.
[77] A. Nourbakhsh, C. Adelmann, Y. Song, C. S. Lee, I. Asselberghs, C. Huyghebaert, S. Brizzi, M. Tallarida, D. Schmeißer, S. Van Elshocht, M. Heyns, J. Kong, T. Palacios, S. De Gendt, *Nanoscale* **2015**, *7*, 10781.
[78] W. C. Shin, J. H. Bong, S.-Y. Choi, B. J. Cho, *ACS Appl. Mater. Interfaces* **2013**, *5*, 11515.
[79] A. Nath, B. D. Kong, A. D. Koehler, V. R. Anderson, V. D. Wheeler, K. M. Daniels, A. K. Boyd, E. R. Cleveland, R. L. Myers-Ward, D. K. Gaskill, K. D. Hobart, F. J. Kub, G. G. Jernigan, *Appl. Phys. Lett.* **2017**, *110*, 13106.
[80] J. E. Johns, J. M. P. Alaboson, S. Patwardhan, C. R. Ryder, G. C. Schatz, M. C. Hersam, *J. Am. Chem. Soc.* **2013**, *135*, 18121.
[81] V. Wheeler, N. Garces, L. Nyakiti, R. Myers-Ward, G. Jernigan, J. Culbertson, C. Eddy, D. Kurt Gaskill, *Carbon* **2012**, *50*, 2307.
[82] L. Zheng, X. Cheng, D. Cao, G. Wang, Z. Wang, D. Xu, C. Xia, L. Shen, Y. Yu, D. Shen, *ACS Appl. Mater. Interfaces* **2014**, *6*, 7014.
[83] L. Zheng, X. Cheng, Y. Yu, Y. Xie, X. Li, Z. Wang, *Phys. Chem. Chem. Phys.* **2015**, *17*, 3179.
[84] K. Jiao, X. Wu, C. Duan, D. Zhang, Y. Wang, Y. Chen, *Phys. Chem. Chem. Phys.* **2015**, *17*, 4757.
[85] N. Y. Garces, V. D. Wheeler, J. K. Hite, G. G. Jernigan, J. L. Tedesco, N. Nepal, C. R. Eddy, D. K. Gaskill, *J. Appl. Phys.* **2011**, *109*, 124304.
[86] Y. Zhang, Q. Fu, Y. Cui, R. Mu, L. Jin, X. Bao, *Phys. Chem. Chem. Phys.* **2013**, *15*, 19042.
[87] Q. Wu, Y. Wu, Y. Hao, J. Geng, M. Charlton, S. Chen, Y. Ren, H. Ji, H. Li, D. W. Boukhvalov, R. D. Piner, C. W. Bielawski, R. S. Ruoff, *Chem. Commun.* **2013**, *49*, 677.
[88] Y.-C. Lin, C.-C. Lu, C.-H. Yeh, C. Jin, K. Suenaga, P.-W. Chiu, *Nano Lett.* **2012**, *12*, 414.
[89] E. Färm, M. Kemell, M. Ritala, M. Leskelä, *J. Phys. Chem. C* **2008**, *112*, 15791.
[90] G. Dingemans, F. Einsele, W. Beyer, M. C. M. van de Sanden, W. M. M. Kessels, *J. Appl. Phys.* **2012**, *111*, 93713.
[91] R. H. J. Vervuurt, A. Sharma, Y. Jiao, W. (Erwin) M. M. Kessels, A. A. Bol, *Nanotechnology* **2016**, *27*, 405302.
[92] Y. Zhou, C. L. Muhich, B. T. Neltner, A. W. Weimer, C. B. Musgrave, *J. Phys. Chem. C* **2012**, *116*, 12114.
[93] P. Wynblatt, N. A. Gjostein, *Acta Metall.* **1976**, *24*, 1165.
[94] A. J. M. Mackus, M. A. Verheijen, N. Leick, A. A. Bol, W. M. M. Kessels, *Chem. Mater.* **2013**, *25*, 1905.
[95] H. G. Zhang, J. T. Sun, T. Low, L. Z. Zhang, Y. Pan, Q. Liu, J. H. Mao, H. T. Zhou, H. M. Guo, S. X. Du, F. Guinea, H.-J. Gao, *Phys. Rev. B* **2011**, *84*, 245436.
[96] A. Konar, T. Fang, D. Jena, *Phys. Rev. B* **2010**, *82*, 115452.
[97] L. A. Ponomarenko, R. Yang, T. M. Mohiuddin, M. I. Katsnelson, K. S. Novoselov, S. V. Morozov, A. A. Zhukov, F. Schedin, E. W. Hill, A. K. Geim, *Phys. Rev. Lett.* **2009**, *102*, 206603.
[98] D. B. Farmer, R. G. Gordon, *Nano Lett.* **2006**, *6*, 699.
[99] C. J. Tainter, G. C. Schatz, *J. Phys. Chem. C* **2016**, *120*, 2950.
[100] J. A. Robinson, M. LaBella, M. Zhu, M. Hollander, R. Kasarda, Z. Hughes, K. Trumbull, R. Cavalero, D. Snyder, *Appl. Phys. Lett.* **2011**, *98*, 53103.
[101] B. M. Foley, S. C. Hernández, J. C. Duda, J. T. Robinson, S. G. Walton, P. E. Hopkins, *Nano Lett.* **2015**, *15*, 4876.
[102] D. W. Yue, C. H. Ra, X. C. Liu, D. Y. Lee, W. J. Yoo, *Nanoscale* **2015**, *7*, 825.
[103] N. F. W. Thissen, R. H. J. Vervuurt, A. J. M. Mackus, J. J. L. Mulders, J.-W. Weber, W. M. M. Kessels, A. A. Bol, *2D Mater.* **2017**, *4*, 25046.

 © 2017 WILEY-VCH Verlag GmbH & Co. KGaA, Weinheim